Zircon LA-ICPMS geochronology of the Cornubian Batholith, SW England

ERIKA R. NEACE[1], R. DAMIAN NANCE[1]*, J. BRENDAN MURPHY[2], PENELOPE J. LANCASTER[3] & ROBIN K. SHAIL[4]

[1]*Department of Geological Sciences, Ohio University, Athens, Ohio 45701, USA*

[2]*Department of Earth Sciences, St. Francis Xavier University, Antigonish, NS, B2G 2W5, Canada*

[3]*School of Earth and Environmental Sciences, University of Portsmouth, Portsmouth PO1 3QL, UK*

[4]*Camborne School of Mines, College of Engineering, Mathematics & Physical Sciences, University of Exeter, Penryn Campus, Penryn, TR10 9FE, UK*

**Corresponding author (e-mail: nance@ohio.edu)*

Abstract

Available U–Pb age data for the Cornubian Batholith of SW England is based almost entirely on monazite and xenotime, and very little zircon U–Pb age data has been published. As a result, no zircon inheritance data is available for the batholith, by which the nature of the unexposed basement of the Rhenohercynian Zone in SW England might be constrained.

Zircon LA-ICPMS data for the Cornubian Batholith provides Concordia ages (Bodmin Moor granite: 316 ± 4 Ma, Carnmenellis granite: 313 ± 3 Ma, Dartmoor granite: ~310 Ma, St. Austell granite: 305 ± 5 Ma, and Land's End granite: 300 ± 5 Ma) that are consistently 20-30 Ma older than previously published emplacement ages for the batholith and unrealistic in terms of geologic relative age relationships with respect to the country rock. This discrepancy is likely as a consequence of minor pre-granitic Pb inheritance. Several of the batholith's granite plutons

contain a component of late-Devonian inheritance that may record rift-related, lower crustal melting or arc-related magmatism associated with subduction of the Rheic Ocean. In addition, the older granites likely contain Mesoproterozoic inheritance, although the highly discordant nature of the Mesoproterozoic ages precludes their use in assigning an affinity to the Rhenohercynian basement in SW England.

Keywords: Cornubian Batholith, zircon geochronology

Introduction

SW England is host to a variety of Palaeozoic igneous and metasedimentary rocks, the complex tectonic history of which is related to the Devonian-Carboniferous closure of the Rheic Ocean (e.g., Floyd et al., 1993; Leveridge & Hartley, 2006; Shail & Leveridge, 2009). Assigned to the European Rhenohercynian Zone (Fig. 1a), these rocks are thought to represent the northern (Avalonian) margin of the Rheic Ocean and their deformation reflects the Variscan collision between Gondwana and Laurussia (e.g., Nance et al., 2010). The Cornubian Batholith, one of the largest granite bodies in the United Kingdom, was emplaced into these deformed Devonian and Carboniferous rocks following the cessation of Variscan convergence. It underlies much of the counties of Cornwall and Devon, and crops out in six major plutons and a larger number of smaller, satellite bodies that extend at least 250 km WSW from Dartmoor to west of the Isles of Scilly (Edmonds et al., 1975; Floyd, et al., 1993).

The Cornubian Batholith and adjacent country rocks host a variety of magmatic-hydrothermal mineral deposits that have been exploited since antiquity (e.g., Penhallurick, 1986), primarily for tin and copper, but also tungsten, arsenic, zinc, silver, cobalt, lead and other

47 metals (Dines, 1956; Le Boutillier, 2003). The area is frequently used as a model for magmatic-
48 hydrothermal vein mineralization (e.g., Dewey, 1925; Hosking, 1950, 1962; Hawkes, 1974;
49 Moore, 1975; Darbyshire & Shepherd, 1985; Jackson et al., 1989) and has contributed
50 significantly to the understanding of ore forming processes.

51 The batholith is considered to have been emplaced during the Early Permian based on
52 both Rb/Sr data (ca. 280-290 Ma; Darbyshire & Shepherd, 1985) and the U–Pb ages of
53 monazite and xenotime (ca. 274-294 Ma; Chesley et al., 1993; Chen et al., 1993). However,
54 because the granites are S-type and were produced by melting of a source with a significant
55 sedimentary component, these early U–Pb isotopic studies largely avoided analyzing zircons,
56 since they were expected to contain a major inherited component. As a result, little is known of
57 the zircon geochronology of the batholith and no data is available on the nature of its crustal
58 source as revealed by zircon inheritance.

59 We present here the results of a new U–Pb LA-ICPMS study of igneous zircons from
60 each of the five major mainland plutons of the Cornubian Batholith and discuss the implications
61 of these data for the age and inheritance of the batholith.

62

63 **Regional Setting**

64 The geology of SW England is dominated by Devonian and Carboniferous sedimentary
65 strata and minor rift-related volcanic units that together constitute a passive margin succession
66 within the European Rhenohercynian zone (Holder & Leveridge, 1986; Matte, 2001; Shail &
67 Leveridge, 2009; Nance et al., 2010; Strachan et al., 2014). This zone, which is thought to be
68 floored by Avalonian crust (Franke, 2000; Matte, 2001; Landing 2004), extends from the
69 Bohemian massif of central Europe (Franke, 1989), westwards through SW England (Floyd,

1993; Shail & Leveridge, 2009) around the Ibero-Armorican arc to lithologically similar rocks in the South Portuguese Zone of southern Iberia that are traditionally correlated with those of SW England (Andrews et al., 1982; Matte, 1986; Franke, 1989; Eden & Andrews, 1990; Floyd et al., 1993; von Raumer et al., 2003; Braid et al., 2012).

In SW England, the succession was likely developed in a marginal basin on the northern flank of the Rheic Ocean (e.g., Shail & Leveridge, 2009), and was deformed and metamorphosed at low- to medium-grade during the late Devonian-early Carboniferous when closure of the Rheic Ocean, as a result of its subduction beneath Avalonia (e.g., Quesada, 1998; Nance et al., 2010; Braid et al., 2011), led to the development of a north-vergent Variscan fold-thrust belt (Edmonds et al., 1975; Shackleton et al., 1982; Franke, 1989). The succession is overthrust by the ca. 397 Ma (Clark et al., 1998) Lizard ophiolite to the south, and is post-tectonically intruded by the early Permian (ca. 274-294 Ma; Chen et al., 1993; Chesley et al., 1993) plutons of the Cornubian Batholith, the generation and emplacement of which was contemporaneous with extensional reactivation of the Rhenohercynian suture (Holder & Leveridge, 1994; Shail & Wilkinson, 1994; Shail & Alexander, 1997; Shail et al., 2003; Shail & Leveridge, 2009).

Cornubian Batholith

The most voluminous igneous rocks of SW England are the granites of the Cornubian Batholith. These underlie the counties of Devon and Cornwall and form part of a single, post-orogenic batholith within the external zone of the Variscan fold-thrust belt (Floyd et al, 1993; Le Boutillier, 2003). The batholith is exposed as an ENE-trending array of plutons that extends at least 250 km and includes (from east to west) the granites of Dartmoor, Bodmin Moor, St.

93 Austell, Carnmenellis, Land's End and the Isles of Scilly (Chen et al., 1993; Chesley et al.,
94 1993) (Fig. 1b). The plutons crosscut the metasedimentary rocks of the Rhenohercynian passive
95 margin succession following their deformation during Variscan convergence (Exeley & Stone,
96 1982; Chappell & Hine, 2006). The youngest deformed strata are Pennsylvanian (Moscovian)
97 approximately 307-315 Ma in age (Gradstein et al., 2012).

98 The batholith is traditionally interpreted to be the product of crustal thickening caused
99 by the collision of Gondwana and Laurussia (Floyd et al, 1993), which closed the Rheic Ocean
100 and led to the formation of Pangaea (e.g., Nance et al., 2010). A predominantly lower crustal
101 source for the peraluminous granites is supported by initial $^{87}Sr/^{86}Sr$ ratios of 0.710–0.716 and
102 εNd values that range from -4.7 to -7.1 (Darbyshire & Shepherd, 1994); a minor mantle
103 component is suggested by εNd data, enclave compositions (Stimac et al., 1995) and the spatial
104 association of the batholith with coeval lamprophyres (Leat et al., 1987; Thorpe, 1987) recently
105 dated ($^{40}Ar/^{39}Ar$ on phlogopite) at between ca. 293.6 and 285.4 Ma (Dupuis et al., 2015). The
106 basement underlying the batholith is unexposed, but is widely considered to be Avalonian
107 (Franke, 1989; von Raumer et al., 2003) and part of the lower plate relative to the SE-dipping
108 Rhenohercynian / Rheic suture imaged on offshore deep seismic reflection profiles (Shail &
109 Leveridge, 2009).

110 More recent work indicates that Early Permian granite emplacement and mineralization
111 primarily occurred during the latter stages of a regional NNW-SSE extensional regime (D_3) that
112 succeeded Variscan convergence in the latest Carboniferous (Alexander & Shail, 1995, 1996;
113 Shail & Alexander, 1997; Shail & Leveridge, 2009). Extensional reactivation of the
114 Rhenohercynian suture brought about exhumation of the lower plate (SW England) and was
115 accompanied by mantle partial melting. The resultant underplating and/or lower crustal

116 emplacement of lamprophyric and basaltic magmas into an already hot lower crust was
117 sufficient to initiate substantial crustal partial melting (Shail & Wilkinson, 1994; Shail et al.,
118 2003). Charoy (1986) concluded that anatexis occurred by partial melting of pelitic rocks at
119 approximately 7-8 kbar and 800 °C in the lower or intermediate crust.

120 Based on gravity modeling, the batholith has a tabular shape originally estimated to be
121 ~13.5 km thick (Willis-Richards & Jackson, 1989). More recently, the thickness has been
122 revised to 5-8 km for the Bodmin Moor, St. Austell and Carnmenellis granites and 10 km for
123 the Dartmoor granite (Taylor, 2007), resulting in an estimated batholith volume of 40,000 km^3
124 (Williamson et al., 2010).

125 The batholith has been extensively studied in connection with fractionated, high-grade,
126 high heat-flow granitic terranes and as a model for tin mineralization and late-stage alteration
127 associated with acidic magmatism (Floyd et al., 1993). It has been heavily mineralized as the
128 result of hydrothermal activity (Dines, 1986; Floyd et al, 1993; Chen et al., 1993), producing
129 many mineral ores that have been extensively mined for millennia (Penhallurick, 1986).

130 Available age data for the Cornubian Batholith includes Rb/Sr geochronology by
131 Darbyshire & Shepherd (1985, 1987), and U–Pb and $^{40}Ar/^{39}Ar$ dating by Chesley et al. (1993),
132 Chen et al. (1993). Based on Rb/Sr data, Darbyshire & Shepherd (1985) placed granite
133 emplacement at ca. 290-280 Ma. Chesley et al. (1993), using U–Pb on monazite and xenotime,
134 and $^{40}Ar/^{39}Ar$ on muscovite and biotite, obtained emplacement ages of ca. 275-300 Ma. Chen et
135 al. (1993) obtained similar results using U–Pb on monazite and $^{40}Ar/^{39}Ar$ on muscovite and
136 biotite. Their data, along with Clark et al. (1994) suggested that the emplacement of the plutons
137 of the Cornubian Batholith was diachronous and ranged in age from 293.1 ± 1.3 Ma
138 (Carnmenellis granite) to 275 ± 1.4 Ma (Land's End granite). Published zircon age data is

limited to three discordant $^{206}Pb/^{238}U$ ages in the range 276-281 Ma from the St. Austell granite (Chesley et al., 1993).

Methods

Approximately 10 kg of rock were collected from each of the five mainland plutons (Dartmoor, Bodmin Moor, St. Austell, Carnmenellis and Land's End) of the Cornubian Batholith and prepared at the University of Portsmouth (UoP), UK. Thin sections for each pluton were made at UoP, then photographed and point-counted at 0.3 mm intervals using a Nikon Labophot2 petrographic microscope at Morehead State University in Morehead, Kentucky, USA.

Zircons were separated from each sample using traditional methods at UoP. After jaw-crushing, the 400–75 μm size fraction was collected after disk milling at the British Geological Survey, Nottingham, UK. Further processing through a Wilfley table, Frantz magnetic separator and LST Fastfloat heavy liquid separation isolated the heavy mineral fraction. Zircons were then hand-picked, mounted into epoxy, and polished to half-height. Each grain was examined in cathodoluminescence (CL) imaging using a JEOL JSM-6060LV scanning electron microscope to identify relevant growth zoning and contaminating features (e.g., cracks or inclusions).

U–Pb ages were measured by laser ablation quadrupole inductively coupled plasma mass spectrometry (LA-Q-ICP-MS) at UoP following Jeffries et al. (2003), using an Agilent 7500cs coupled to a New Wave Research UP-213 Nd:YAG laser. A 30 μm spot was rastered along a 45–60 μm line. Grains were analyzed using the ribbon method to avoid any analytical bias towards 'nice' grains (e.g., Mange & Maurer, 1992).

161 Ratios were calculated using an in-house spreadsheet based on LamTool (Košler et al.,
162 2008), normalized to GJ-1. All uncertainties were propagated in quadrature and no common Pb
163 correction was undertaken. Average $^{206}Pb/^{238}U$ and $^{207}Pb/^{206}Pb$ ratios for GJ-1 were
164 0.09760±0.00197 and 0.06013±0.00145 (n=174, 2SD), respectively, consistent with published
165 values (Jackson et al., 2004). Plešovice, normally measured as the internal standard, was used
166 up shortly before the analyses in this work were undertaken, necessitating the use of GJ-1 as
167 internal standard as well. The resulting $^{206}Pb/^{238}U$ and $^{207}Pb/^{206}Pb$ ratios were 0.09749±0.00193
168 and 0.06009±0.00145 (n=65, 2SD), respectively. In the 11 days prior to this work, analysis of
169 Plešovice as the internal standard yielded $^{206}Pb/^{238}U$ and $^{207}Pb/^{206}Pb$ ratios of 0.05457±0.00270
170 (n=93, 95%) and 0.05342±0.00203 (n=93, 2SD), respectively, consistent with published values
171 (Sláma et al., 2008).
172
173 **Results**
174 U–Pb data are presented in Tables 1–5 and plotted on Concordia diagrams in Figures 4, 8,
175 9, 14, 18, 23. Concordia ages were calculated from concordant (calculated concordance between
176 80–120%) rim and whole grain analyses, interpreted to record the same growth zone event. A
177 Concordia age for the Dartmoor sample could not be calculated due to an insufficient number of
178 concordant rim analyses. Instead, all data from this sample are plotted to indicate the overall
179 discordant array which intersects the Concordia curve at ~310 Ma.
180 The Land's End sample was of a fine-grained muscovite-biotite granite. In thin-section,
181 several instances of oxidation were noted and nearly all feldspar grains were heavily sericitised.
182 Chlorite was also present, probably replacing biotite. No evidence of substantial weathering or
183 alteration was noted in the thin sections for any of the other four plutons. The Carnmenellis,

184 Bodmin Moor, Dartmoor, and St. Austell granite thin sections were all of coarse-grained
185 megacrystic biotite granite, which is consistent with other mineralogical studies of the
186 Cornubian Batholith (Hawkes & Dangerfield, 1978; Dangerfield & Hawkes, 1981). The large
187 grain sizes of these four plutons resulted in count totals below 2000, the lowest count being 334
188 for the St Austell granite, which may not have produced an accurate modal percentage or
189 classification for these granites. Biotite megacrysts as large as 5 mm as well as quartz and
190 potassium feldspar megacrysts as large as 6 mm in the form of perthite were present in the St.
191 Austell granite. Megacrysts were slightly smaller in the Carnmenellis, Bodmin Moor and
192 Dartmoor granites, at < 5 mm. The grains for each of these four plutons were mostly euhedral.
193 A few opaque minerals were found in each of the thin-sections, with the highest modal
194 percentage of 0.74% in the St. Austell granite and the lowest modal percentage of 0.12% in the
195 Bodmin Moor granite.
196
197 *Dartmoor Granite*
198 Sample EN13DM-MV is a megacrystic biotite granite from Merrivale Quarry (Ordnance
199 Survey grid reference SX 546751) and comprises K-feldspar (22.5%), quartz (39.5%),
200 plagioclase (albite 20.3%), biotite (9.8%), muscovite (6.6%), and accessory sphene, apatite, and
201 zircon. A total of 42 zircon grains were analyzed. Figure 2 displays thin section photos of biotite
202 with halos of radiation damage from zircon grains. In CL these proved to be euhedral or
203 euhedral fragments (most >200 μm in length) with well-defined igneous zoning (Fig. 3). These
204 grains yielded $^{206}Pb/^{238}U$ ages in the range ca. 468-297 Ma (Ordovician-Permian), but all are
205 highly discordant (Table 1). A Concordia plot was not generated because insufficient analyses
206 fitted the criteria for inclusion. This may reflect some disturbance of the granite, evidenced by

the dark, unzoned rims of the zircon grains from this sample under CL (Fig. 3), as well as the large number of discordant grains. A Tera-Wasserburg plot of the data (Fig. 4) suggests a crystallization age of ca. 310 Ma, although this can only be considered an approximation. Figure 5 is a scatter plot of the Th/U ratios and the $^{206}Pb/^{238}U$ ages for the Dartmoor granite. Th/U ratios for the Dartmoor granite range from 0.05 – 0.7.

Bodmin Moor Granite

Sample EN13BM-DL is a megacrystic biotite granite from the DeLank Quarry (OS grid reference SX 101753) and comprises K-feldspar (20.6 %), quartz (42.3 %), plagioclase (albite 18.2 %), biotite (11.9 %), muscovite (6.9 %), and accessory apatite, with some sericite replacement of albite. A total of 44 zircon grains were analyzed. Figure 6 displays thin section photos where darkened halos within biotite indicate the presence of radioactive zircon grains. In CL these proved to be euhedral and elongate, with lengths ranging from <100 μm to >200 μm and well-defined igneous zonation (Fig. 7). These grains yielded $^{206}Pb/^{238}U$ ages in the range ca. 413-294 Ma (Devonian-Permian), but most are highly discordant (Table 2). Five concordant grains yielded a Concordia age of 316±4 Ma, which is taken as the best estimate for the age of crystallization (Fig. 9). Four concordant zircons with Concordia age of 371.5 ± 12 Ma are interpreted to be inherited (Fig. 8). Figure 10 is a scatter plot of the Th/U ratios and the $^{206}Pb/^{238}U$ ages of the Bodmin Moor granite. Figure 11 is a scatter plot of this data that excludes an extreme Th/U outlier to present a better general representation of this data for the Bodmin Moor granite. Th/U ratios for the Bodmin Moor granite range from 0.1 – 27.5.

St Austell Granite

230 Sample EN13SA-LUX is a megacrystic biotite granite from the Luxulyan Quarry (OS
231 grid reference SX 053590) and comprises K-feldspar (12.9 %), quartz (43.7 %), plagioclase
232 (albite 17.7 %), biotite (11.7 %), muscovite (6.3 %), and accessory apatite, zircon, sphene,
233 cordierite, and chlorite with some sericite replacement of albite. A total of 56 zircon grains were
234 analyzed. Figure 12 displays photos of biotite in thin section with similar dark halos of radiation
235 damage from radioactive zircons to those seen in the Dartmoor and Bodmin Moor granites. In
236 CL these zircons formed elongate euhedral crystals and blocky euhedral grains, ranging in
237 length from <100 μm to >300 μm with clear igneous zonation (Fig. 13). These grains yielded
238 $^{206}Pb/^{238}U$ ages in the range ca. 344-242 Ma (Carboniferous - Triassic), but are mostly highly
239 discordant (Table 3). Nine concordant grains yielded a Concordia age of 305 ± 5 Ma (Fig. 14),
240 which is taken as the best estimate for the age of crystallization. Figure 15 is a scatter plot of the
241 Th/U ratios plotted against the $^{206}Pb/^{238}U$ ages. Th/U ratios for the St Austell granite range from
242 0.04 – 2.3 (Fig. 15).
243
244 *Carnmenellis Granite*
245 Sample EN13CARN-ROSE is a megacrystic biotite granite from the Rosemanowes
246 Quarry (OS grid reference SW 735346) and comprises K-feldspar (25.8 %), quartz (34.7 %),
247 plagioclase (albite 24.4 %), biotite (6.5 %), muscovite (4.8 %), and accessory apatite, zircon,
248 and sphene with some sericite replacement of albite. A total of 43 zircon grains were analyzed.
249 Figure 16 also presents thin section photos that display halos of radiation damage within biotite
250 (Figure 16c is a 40x photo of a zircon grain in cross-section where the halo can be clearly seen).
251 In CL these grains were elongate or blocky, euhedral grains with clear igneous zoning, and
252 ranged in size from <100 μm to >300 μm (Fig. 17). All but two of these grains yielded

253 $^{206}Pb/^{238}U$ ages in the range ca. 573 - 285 Ma (Neoproterozoic - Permian), but most are highly
254 discordant (Table 4). Two grains yielded much older $^{206}Pb/^{238}U$ ages of ca. 928 and 1631 Ma,
255 indicating inheritance. Eight concordant grains yielded a Concordia age of 313 ± 3 Ma (Fig.
256 18), which is taken as the best estimate for the age of crystallization. Th/U ratios for the
257 Carnmenellis granite range from 0.01 – 1.7 (Figs. 19, 20). Figure 19 includes the zircons that
258 are interpreted to be inherited to display all of the data used for the Carnmenellis granite. Figure
259 20 excludes the two inherited ages so that the relationship between the remaining grains can be
260 seen more clearly.
261
262 *Land's End Granite*
263 Sample EN13LE-CAD is a fine-grained biotite-muscovite granite from the Castle-an-
264 Dinas Quarry (OS grid reference SW 484343) and comprises K-feldspar (23.7 %), quartz (38.8
265 %), plagioclase (albite 22.6 %), biotite (7.1 %), muscovite (6.8 %) and accessory zircon,
266 sphene, cordierite and chlorite, with significant sericite replacement of feldspar. Figure 21
267 shows thin section photos of the Land's End granite, although no halos of radiation damage
268 were observed in thin section. The sample yielded only 5 zircon grains. In CL (Fig. 22) these
269 proved to be either small, elongate euhedral grains or large, blocky euhedral grains, with sizes
270 ranging between 100 μm and 200 μm. Igneous zoning is clearly apparent in the larger grains.
271 These grains yielded $^{206}Pb/^{238}U$ ages in the range ca. 334-294 Ma (Carboniferous - Permian),
272 but most are highly discordant (Table 5). Three concordant grains yielded a Concordia age of
273 300 ± 5 Ma (Fig. 23), which is taken as the best estimate for the age of crystallization. Figure 24
274 is a scatter plot of the Th/U ratios and the $^{206}Pb/^{238}U$ ages for the Land's End granite, although

the small number of analyses for this granite may not be entirely representative of the zircon population. Th/U ratios for the Land's End granite range from 0.1 – 0.4.

Discussion

Comparison with TIMS U–Pb monazite/xenotime data

In Figure 25, the LA-ICPMS U–Pb zircon ages from this study are presented as relative age probability plots in order to summarize the results and highlight variations between the five plutons. The age data are then compared to the TIMS U–Pb monazite and xenotime ages from identical or similar locations reported by Chen et al. (1993) and Chesley et al. (1993) summarized in Table 6 and Figure 26. There is generally a very close agreement between the TIMS U–Pb monazite and xenotime ages for the Carnmenellis, Land's End and St Austell plutons in these independent earlier studies. In addition, the $^{40}Ar/^{39}Ar$ muscovite and biotite cooling ages across these and other plutons of the Cornubian Batholith were shown by both studies to be consistently 3-5 Ma younger than the corresponding U–Pb monazite/xenotime magmatic ages (Chen et al., 1993; Chesley et al., 1993). The U–Pb monazite age of 281 Ma for the Bodmin Moor granite reported by Chen et al. (1993) is anomalously young (less than the corresponding muscovite cooling age), and the 291 Ma U–Pb monazite age of Chesley et al. (1993) is considered more reliable.

Based on the U–Pb zircon Tera-Wasserburg plots (Figs. 4, 8, 9, 14, 18, 23) the five mainland plutons of the batholith are, in order of decreasing age, Bodmin Moor (316 ± 4 Ma, MWSD = 1.2), Carnmenellis (313 ± 3 Ma, MWSD = 0.88), Dartmoor (approx. 310 Ma), St. Austell (305 ± 5 Ma, MSWD = 2.1), and Land's End (300 ± 5 Ma, MWSD = 1.3). The U–Pb zircon data support the U–Pb monazite and xenotime data of Chen et al. (1993) and Chesley et

298 al. (1993) in suggesting that emplacement of the Cornubian Batholith occurred diachronously.
299 However, whilst there is little evidence of inheritance in the data used to construct the
300 Concordia plots – only those zircon analyses showing no indication of common Pb
301 contamination or Pb loss were included – the zircon ages are consistently 20-30 Ma older than
302 the corresponding U–Pb monazite ages (Fig. 26). The discrepancy between the zircon and
303 monazite age data is a systematic one in that both data sets indicate the Land's End pluton to be
304 the youngest of the five, and the Bodmin Moor and Carnmenellis plutons to be the oldest.

305 A possible explanation for this age discrepancy is the lower closure temperature of
306 monazite ($\geq 750^{o}C$; Dahl, 1997) versus that of zircon and xenotime ($\geq 900^{o}C$; Dahl, 1997; Liu
307 et al., 2011), which might be expected to produce monazite ages that are slightly younger than
308 the zircon ages from the same granitic body because of the greater length of time required for
309 the monazites to cool to their closure temperature. However, such an explanation would require
310 the magma to have had an unreasonably long crustal residence time of 20-25 Ma.

311 In many other studies, zircon and monazite ages from the same granite agree within
312 analytical uncertainties (e.g., Kusiak et al., 2014), and some experiments suggest that the
313 closure temperature for Pb in zircon could be similar to that of monazite (e.g., Cherniak and
314 Watson 2003). Indeed, Chesley et al. (1993) presented U–Pb analyses for three zircon fractions
315 from the St Austell granite that indicated broadly similar ages (278-284 Ma) to those of
316 monazites from the same sample (282 Ma). Nevertheless, all of these zircons were discordant
317 and their $^{207}Pb/^{206}Pb$ ages ranged between 307-292 Ma, which Chesley et al. (1993) interpreted
318 to be a consequence of the inheritance of pre-granitic Pb.

319 However, it can be shown on the basis of field relations that the older emplacement ages
320 are geologically unrealistic. Outcrop relations across SW England indicate that emplacement of

321 the Cornubian Batholith post-dated structures developed during both Variscan convergence and
322 the initial stages of post-Variscan extensional reactivation of major thrust faults (Alexander &
323 Shail, 1995; 1996; Shail & Alexander, 1997; Shail & Leveridge, 2009). The LA-ICPMS U–Pb
324 zircon ages of the oldest (ca. 313-316 Ma) plutons overlap or slightly pre-date the depositional
325 age (ca. 307-315 Ma; Gradstein et al., 2012) of the youngest (Moscovian) metasedimentary
326 strata (Bude Formation) in the Culm Basin that was intruded by the batholith. These strata could
327 not undergo Variscan convergence-related deformation (resulting in 6-8 km of tectonic burial),
328 followed by post-Variscan extension and exhumation prior to granite emplacement on a
329 timescale that would render such zircon ages realistic. This implies that the zircon ages are too
330 old. Furthermore, the Crediton Graben, locally developed upon the exhumed Culm Basin, is
331 infilled by a latest Carboniferous-Early Permian red-bed succession containing lamprophyre
332 lavas towards its base dated at 290.8 ± 0.8 Ma (Edwards et al., 1997), that are a robust indicator
333 of the earliest post-Variscan magmatism in the region (e.g., Dupuis et al., 2015).
334 Figure 25 also displays the major tectonic and structural events that are directly related
335 to the emplacement of the Cornubian Batholith (i.e., the closure of the Rheic Ocean and the
336 resultant Variscan orogeny, the obduction of the Lizard Ophiolite, extension and reactivation of
337 the Rhenohercynian Suture). The highest age probability for all of the granites except Land's
338 End occurs before the period of extension that preceded granite emplacement, during the
339 closure of the Rheic Ocean. Therefore these ages cannot represent the age of emplacement for
340 the granites. Given that the U–Pb zircon Concordia age data reported here can be shown to be
341 anomalously old, the age discrepancy is likely to be a consequence of minor pre-granitic Pb
342 inheritance.
343 *Zircon inheritance in the Cornubian Batholith*

It is surprising that the U–Pb analyses of zircons from the Cornubian Batholith, taken as a whole, provide so little evidence of pre-Permian inheritance. The reason for this paucity of older zircons is uncertain since it is unlikely that entire age populations were missed by our sampling and all indications point to the Cornubian Batholith biotite granites as having been produced by melting of a source with an overwhelming crustal component (e.g. Charoy, 1986; Darbyshire & Shepherd, 1994; Chappell & Hine, 2006). Miller et al. (2003) have suggested that inheritance-poor granites are indicative of high-temperature (>800 ^{o}C) magma generation and suggest a magma source that may have been undersaturated with zircon. They also noted that completely inheritance-free granites are always metaluminous or weakly peraluminous, whereas a few of those with minor inherited zircon and the majority of those with significant inherited zircon are strongly peraluminous. Table 7 presents the whole-rock geochemistry data of Stone (2000) for inner and outer granite samples of the Bodmin Moor and Carnmenellis granites. Stone (2000) defines the boundary between the inner and outer granites as the point where $tFe_2O_3 + MgO = 1.8$ wt%. These data are used to calculate the variable *M* in the equation for zircon solubility established by Watson & Harrison (1983):

$$\left(lnD_{Zr}^{\frac{zircon}{melt}} = \{-3.8 - [0.85(M-1)]\} + \frac{12900}{T}\right), \qquad \text{(Eq. 1)}$$

where *M* is a cation ratio accounting for the dependence of zircon solubility upon SiO_2 and peraluminosity of the melt:

$$M = \left(\frac{Na + K + 2Ca}{Al \cdot Si}\right), \qquad \text{(Eq. 2)}$$

and *T* is temperature in degrees kelvin. Using this data and solving for *T* (e.g., Miller et al., 2003):

$$T_{Zr} = \left(\frac{12900}{2.95 + 0.85M + \ln\left(\frac{496000}{Zr_{melt}}\right)} \right) \quad \text{(Eq. 3)}$$

the geothermometer for zircon saturation temperatures in the Bodmin Moor and Carnmenellis granites were calculated (see Table 7) resulting in T_{Zr} temperatures of 727 – 775 °C. According to Miller et al. (2003), T_{Zr} values of 730-780 °C should represent granites with a strong inherited zircon component.

However, zircon inheritance is not entirely absent. A few strongly discordant zircon grains give Mesoproterozoic $^{207}Pb/^{206}Pb$ ages, although these give no indication as to the nature of the basement and whether or not it has Avalonian affinities. Nance et al. (2015) discuss the possibility that the underlying, unexposed basement of SW England could be a correlative of the Meguma terrane rather than the traditionally assigned Avalon terrane (Franke, 2000; Matte, 2001; Landing 2004; Shail & Leveridge, 2009). While the two discordant Mesoproterozoic ages from this study alone cannot be used to make any suggestion about the nature of the unexposed basement, a few studies have been conducted which provide some limited insight into the basement of SW England. Schofield et al. (2010) also regressed one highly discordant zircon age with a Mesoproterozoic upper limit age of 1648 Ma in the Stanner Hanter complex (Wales, UK). Sandeman et al. (2000) conducted U–Pb analysis of the Kennack Gneiss (which intrudes the Lizard ophiolite to the east of the Cornubian Batholith) that resulted in a Concordia upper intercept of 2012 ± 13 Ma and a lower intercept of 376.4 ± 1.7 Ma. They interpreted the lower intercept as representing the age of emplacement of the Kennack Geniss, and suggested that the upper intercept might correspond to the approximate age of the ancient source of the melt. Their Concordia results were produced from four zircon grains, one highly discordant grain providing a Mesoproterozoic $^{207}Pb/^{206}Pb$ age of 1389.2 Ma. Although all of these Mesoproterozoic ages

387 are highly discordant, they document the presence of ancient crustal material in each of these
388 bodies.

389 Some of the granites, in particular the older plutons, contain a significant component of
390 late Devonian (Frasnian/Famennian) inherited zircons. This is most clearly evident in the 372 ±
391 12 Ma (MWSD = 1.2) age of the older Concordia plot from the Bodmin Moor granite (Fig. 8).
392 The source of this late Devonian inheritance is problematic since the only exposed igneous
393 rocks of this age in SW England are mafic and thought to be rift-related (Merriman et al., 2000;
394 Shail & Leveridge, 2009), and so are unlikely to contain zircons. It is possible, however, that
395 the zircons were formed during partial melting of the lower continental crust during this rifting
396 event. However, another potential source of late Devonian zircons would be the arc-related
397 plutons associated with the subduction of the Rheic Ocean beneath Avalonia (e.g., Nance et al.,
398 2010; Braid et al., 2011; Quesada, 1998). These are not exposed in SW England, but occur
399 immediately south of the Rhenohercynian Zone farther east, in the Mid-German Crystalline
400 Rise (Zeh et al., 2001), and farther west, in the South Portuguese Zone of southern Iberia (Braid
401 et al, 2010). Upper Devonian granitoid clasts derived from the equivalent of the Mid-German
402 Crystalline Rise occur in the proximal southerly derived Gramscatho Basin succession
403 immediately north of the Lizard Ophiolite (Dörr et al., 1999), although it is difficult to envisage
404 how such material would be incorporated into the continental crust of the lower plate. It is also
405 possible that the late Devonian ages are artifacts of contamination. For example, there is some
406 indication of disturbance within the Dartmoor granite, evidenced by the presence of unzoned
407 rims on zircon grains and highly discordant age data that may suggest common Pb
408 contamination. But these features are not strongly evident in the other granites.

Th/U ratios in zircon can be used as an indicator of the environment in which zircon grew (Rubatto, 2002; Kirkland et al., 2015). Low Th/U ratios (< 0.1) within zircon can be an indication of metamorphic rather than magmatic growth (Rubatto, 2002), while relatively high Th/U ratios may indicate high-grade metamorphism (Wan et al., 2011). Significant lack of zoning within zircon can also indicate metamorphic growth. The Dartmoor granite showed poor zoning in CL, and in seven analyses Th/U ratios were less than 0.1. It is well known that the Cornubian Batholith has been hydrothermally altered, such that metamorphic minerals might be expected to produce ages that are younger than the age of crystallization. Yet the estimated age of 310 Ma for the Dartmoor granite presented here is 30 Ma older than the ~280 Ma ages reported by Chen et al. (1993) and Chesley et al. (1993). The Bodmin Moor granite has Th/U ratios that range between 0.1 – 2.3, with an outlier of 27.5. The St. Austell, Carnmenellis, and Land's End granites respectively record five, three, and two analyses with Th/U ratios of less than 0.1. The Land's End granite produced the only scatter plot of Th/U ratios vs. $^{206}Pb/^{238}U$ ages (Figs. 5, 10, 11, 15, 19, 20, 24) with an R^2 value greater than 0.5, and only the Bodmin Moor plot that excludes an outlier (Fig. 11) has an R^2 value greater than 0.01. However, the high R^2 value of the Land's End granite may be the result of the limited number of analyses, with only 5 data points, and so may not be an accurate representation of a relationship, or lack thereof, between the Th/U ratios and $^{206}Pb/^{238}U$.

Conclusions

LA-ICPMS U–Pb zircon ages for the Cornubian Batholith match previously published age data in suggesting that the Bodmin Moor and Carnmenellis granites are the oldest plutons while the Land's End granite is the youngest, and that emplacement of the batholith was

diachronous. However, the zircon ages are consistently 20-30 Ma older than previously published U–Pb monazite data (Chen et al., 1993; Chesley et al., 1993). Cross-cutting relations with structures within the batholith's Devonian-Carboniferous host rocks, the depositional age of which overlaps the reported zircon ages, indicate that the zircon data provide unrealistic emplacement ages.

U–Pb analysis of zircons from the Cornubian Batholith provide little evidence of pre-Permian inheritance. The reasons for this scarcity are uncertain, although inheritance is not entirely absent. Several plutons contain a component of late Devonian inheritance, the source of which is problematic since the only exposed igneous rocks of Devonian age in SW England are mafic and are considered to be rift-related (Merriman et al., 2000; Shail & Leveridge, 2009). The inheritance may record lower crustal melting during this rifting event, or may be linked to arc-related magmatism that has been associated with subduction of the Rheic Ocean elsewhere in the Rhenohercynian Zone.

These data also include a few grains with Mesoproterozoic $^{207}Pb/^{206}Pb$ ages, although these are too discordant to be used to assess the nature of the basement and whether or not it is of Avalonian affinity. However, together with other studies in southern Britain that have produced highly discordant Mesoproterozoic zircon ages they do indicate the presence of an ancient crustal component in the igneous rocks of SW England.

Acknowledgements

This project was supported by the Department of Geological Sciences at Ohio University and by NSERC (Canada) through Discovery grants to JBM. Thanks are also extended to the faculty and staff in the School of Earth and Environmental Sciences at the

University of Portsmouth, the British Geological Survey, and the Department of Earth Systems Science at Morehead State University for the use of their facilities. Thoughtful reviews by Mike Searle and an anonymous reviewer greatly improved the final manuscript.

References

Alexander, A.C., Shail, R.K. (1995). Late Variscan structures on the coast between Perranporth and St. Ives, south Cornwall. *Proceedings of the Ussher Society, 8*, 398-404.

Alexander, A.C., Shail, R.K. (1996). Late- to Post-Variscan structures on the coast between Penzance and Pentewan, south Cornwall. *Proceedings of the Ussher Society, 9*, 72-78.

Andrews, J.R. (1982). The Iberian Pyrite Belt, south-west England and Hercynian geotectonics. *Proceedings of the Ussher Society, 5,* 387-389.

Barbarin, B. (1996). Genesis of the two main types of peraluminous granites. *Geology, 24,* 295.

Braid, J., Murphy, J., Quesada, C. (2010). Structural analysis of an accretionary prism in a continental collision setting, the Late Paleozoic Pulo do Lobo Zone, Southern Iberia. *Gondwana Research,17*, 422-439.

Braid, J., Murphy, J., Quesada, C., Mortensen, J. (2011). Tectonic escape of a crustal fragment during the closure of the Rheic Ocean: U–Pb detrital zircon data from the Late Paleozoic Pulo do Lobo and South Portuguese zones, southern Iberia. *Journal of the Geological Society, London , 168*, 383-392. http://dx.doi.org/10.1144/0016-76492010-104

Braid, J., Murphy, B., Quesada, C., Bickerton, L., Mortensen, J. (2012). Probing the composition of unexposed basement, South Portuguese Zone, southern Iberia: implications for the connections between the Appalachian and Variscan orogens. *Canadian Journal of Earth Sciences , 49*, 591-613. http://dx.doi.org/10.1139/e11-071

478 Chappell, B.W., Hine, R. (2006). The Cornubian Batholith: an example of magmatic
479 fractionation on a crustal scale. *Resource Geology, 56,* 203-244.
480 Charoy, B. (1986). The genesis of the Cornubian batholith (South-west England): the example
481 of the Carnmenellis pluton. *Journal of Petrology, 27*, 571-604.
482 Chen, Y., Clark, A., Farrar, E., Wasteneys, H., Hodgson, M., Bromley, A. (1993). Diachronous
483 and independent histories of plutonism and mineralization in the Cornubian Batholith,
484 southwest England. *Journal of the Geological Society, London* 150, 1183-1191.
485 Cherniak, D.J., Watson, E.B. (2003). Diffusion in Zircon. *Reviews in Mineralogy and*
486 *Geochemistry* 53, 113-143.
487 Chesley, J.T., Halladay, A.N., Snee, L.W., Mezger, K., Shepherd, T.J., Scrivener, R.C. (1993).
488 Thermochronology of the Cornubian batholith in southwest England: Implications for
489 pluton emplacement and protracted hydrothermal mineralization. *Geochimica et*
490 *Cosmochimica Acta, 57*, 1817-1835.
491 Clark, A.H., Chen, Y., Farrar, E., Northcote, B., Wastenays, H.A.H.P., Hodgson, M.J.,
492 Bromley, A. (1994). Refinement of the time/space relationships of intrusion and
493 hydrothermal activity in the Cornubian Batholith (abstract). *Proceedings of the Ussher*
494 *Society, 8*, 345.
495 Clark, A.H., Sandeman, H.A., Liu, C., Scott, D.J., Farrar, E., Archibald, D.A., Bromley, A.V.,
496 Jones, K.A., Warr, L.N. (1998). An emerging geochronological record of the construction
497 and emplacement of the Lizard Ophiolite, SW Cornwall. *Geoscience of South-West*
498 *England, 9*, 276-277.

499 Dahl, P.S. (1997). A crystal-chemical basis for Pb retention and fission-track annealing
500 systematics in U-bearing minerals, with implications for geochronology. *Earth and*
501 *Planetary Science Letters, 150*, 277-290.
502 Dangerfield, J., Hawkes, J.R. (1981). The Variscan granites of south-west England: additional
503 information. Proceedings of the Ussher Society, 5, 116-120.
504 Darbyshire, D.P.F., Shepherd, T.J. (1985). Chronology of granite magmatism and associated
505 mineralization, SW England. *Journal of the Geological Society of London 142*, 1159-
506 1178.
507 Darbyshire, D.P.F., Shepherd, T.J. (1987). Chronology of magmatism in south-west England:
508 the minor intrusions. *Proceedings of the Ussher Society,* 6, 431-438.
509 Darbyshire, D.P.F., Shepherd, T.J. (1994). Nd and Sr isotope constraints on the origin of the
510 Cornubian batholith, SW England. *Journal of the Geological Society of London, 151*, 795-
511 802.
512 Dewey, H. (1925). The mineral zones of Cornwall. *Proceedings of the Geologists' Association,*
513 *36*, 107-I35.
514 Dines, H.G. (1956). *The metalliferous mining region of south-west England.* Economic Memoir
515 of the Geological Survey of Great Britain.
516 Dörr, W., Floyd, P.A., Leveridge, B.E. (1999). U–Pb ages and geochemistry of granite pebbles
517 from the Devonian Menaver Conglomerate, Lizard peninsula: provenance of
518 Rhenohercynian flysch of SW England. *Sedimentary Geology, 124,* 131-147.
519 Dupuis, N.E., Braid, J.A. Murphy, J.B., Shail, R.K., Archibald, D.A., Nance, R.D. (2015).
520 40Ar/39Ar phlogopite geochronology of lamprophyre dykes in Cornwall, UK: new age

521 constraints on Early Permian post-collisional magmatism in the Rhenohercynian Zone,
522 SW England. *Journal of the Geological Society, 172*, in press.
523 Eden, C.P., Andrews, J.R. (1990). Middle to Upper Devonian melanges in SW Spainand their
524 relationship to the Meneage Formation in south Cornwall. *Proceedings of the Ussher*
525 *Society, 7*, 217-222.
526 Edmonds, E.A., McKeown, M.C., William, M. (1975). British Regional Geology: Southwest
527 England, 4th edition. *BGS Publication*, HMSO, London, 136 p.
528 Edwards, R. A., Warrington, G., Scrivener, R. C., Jones, N.S., Haslam, H. W., Ault, L. (1997).
529 The Exeter Group, south Devon, England: a contribution to the early post-Variscan
530 stratigraphy of northwest Europe. Geological Magazine, 134, 177-197.
531 Floyd, P., Exley, C., Styles, M. (1993). Igneous rocks of south-west England. In: *Geological*
532 *Conservation Review Series, No. 5* (p. 256). London: Chapman and Hall.
533 Franke, W. (1989). Tectonostratigraphic units in the Variscan belt of central Europe. *Geological*
534 *Society of America, Special Paper, 230*, 67-90.
535 Franke, W. (2000). The mid-European segment of the Variscides: tectonostratigraphic units,
536 terrane boundaries and plate tectonic evolution, *in*, Dallmeyer, R.D., Franke, W., and
537 Weber, K., *eds.*, Orogenic Processes: Quantification and Modelling in the Variscan Belt.
538 *Geological Society, London, Special Publications, 179*, 35-61.
539 http://dx.doi.org/10.1144/GSL.SP.2000.179.01.05
540 Gradstein, F.M., Ogg, J.G., Frits J. Hilgen, F.J., 2012. On the Geologic Time Scale. *Newsletters*
541 *on Stratigraphy* 45, 171–188.
542 Hawkes, J.R. (1974). Volcanism and metallogenesis: the tin province of south-west England.
543 *Bulletin Volcanologique, 38*, 1125-1146.

544 Hawkes, J.R., Dangerfield, J. (1978). The Variscan granites of south-west England: a progress
545 report. *Proceedings of the Ussher Society*, 4, 158-171.
546 Holder, M.T., Leveridge, B.E. (1986). Correlation of the Rhenohercynian Variscides. *Journal of*
547 *the Geological Society of London 143*, 141-147.
548 Holder, M.T., Leveridge, B.E. (1994). A framework for the European Variscides. British
549 Geological Survey, Onshore Geology Series, Technical Report WA/94/24. *British*
550 *Geological Survey,* UK, 53 p.
551 Hosking, K.F.G. (1950). Fissure systems and mineralization in Cornwall. *Transactions of the*
552 *Royal Geological Society of Cornwall, 18*, 9-49.
553 Hosking, K.F.G. (1962). The relationship between the primary mineralization and the structure
554 of South-West England. In: *Some Aspects of the Variscan Fold Belt*. Manchester
555 University Press, 135-153.
556 Jackson, N.J., Willis-Richards, J., Manning, D.A.C., Sams, M.S. (1989). Evolution of the
557 Cornubian ore field, southwest England; Part II. Mineral deposits and ore-forming
558 processes. *Economic Geology, 84,* 1101-1133.
559 Jackson, S.E., Pearson, N.J., Griffin, W.L., Belousova, E.A. (2004). The application of laser
560 ablation-inductively coupled plasma-mass spectrometry to *in situ* U–Pb zircon
561 geochronology. *Chemical Geology, 211*, 47-69.
562 Jeffries, T.E., Fernandez-Suarez, J., Corfu, F., Alonso, G.G. (2003). Advances in U–Pb
563 geochronology using a frequency quintupled Nd:YAG laser ablation system ($\lambda = 213$ nm)
564 and quadrupole based ICP-MS. *Journal of Analytical Atomic Spectrometry*, *18*, 847-855.
565 Kirkland, C.L., Smithies, R.H., Taylor, R.J.M., Evans, N., McDonald, B. (2015). Zircon Th/U
566 ratios in magmatic environs. *Lithos, 212-215*, 397-414.

567 Košler, J., Forst, L., Sláma, J. (2008). LamDate and LamTool: Spreadsheet-based Data
568 Reduction for Laser Ablation ICP-MS. In: Sylvester, P.J. (Ed.), Laser ablation in Earth
569 Sciences. *Current practices and outstanding issues, Short Course Series 40*, pp. 315-317.
570 Kusiak, M.A., Williams, I.S., Dunkley, D.J., Konečny, P., Słaby, E., Martin, H. (2014).
571 Monazite to the rescue: U-Th_Pb dating of the intrusive history of the composite
572 Karkonosze pluton, Bohemian Massif. *Chemical Geology, 364*, 76-92.
573 Landing, E. (2004). Precambrian-Cambrian boundary interval deposition and the marginal
574 platform of the Avalon microcontinent. *Journal of Geodynamics, 37*, 411-435.
575 http://dx.doi.org/10.1016/j.jog.2004.02.014
576 Leat, P.T., Thompson, R.N., Morrison, M.A., Hendry, G.L., Trayhorn, S.C. (1987).
577 Geodynamic significance of post-Variscan intrusive and extrusive potassic magmatism in
578 SW England. *Transactions of the Royal Society of Edinburgh: Earth Sciences, 77*, 349-
579 360.
580 Le Boutillier, N. G. (2003). The tectonics of Variscan magmatism and mineralisation in South
581 West England. Unpublished PhD thesis, *University of Exeter*.
582 Leveridge, B. & Hartley, A.J. (2006). The Variscan Orogeny: the development and deformation
583 of Devonian/Carboniferous basins in SW England and South Wales. In: Brenchley, P.J.;
584 Rawson, P.F. (eds.) *The Geology of England and Wales*. London, Geological Society of
585 London, 225-255.
586 Liu, Z.C., Wu, F.Y., Guo, C.L., Zhao, Z.F., Yang, J.H., Sun, J.F. (2011). In situ U-Pb dating of
587 xenotime by laser ablation (LA)-ICP-MS. *Chinese Science Bulletin* 56, 2948-2956. doi:
588 10.1007/s11434-011-4657-y.
589 Mange, M.A., Mauer, H.F.W. (1992). Heavy minerals in colour. *Chapman and Hall, London*.

590 Matte, P. (1986). Tectonics and plate tectonics model for the Variscan belt of Europe.
591 *Tectonophysics, 126*, 329-374. http://dx.doi.org/10.1016/0040-1951(86)90237-4
592 Matte, P. (2001). The Variscan collage and orogeny (480-290 Ma) and the tectonic definition of
593 the Armorica microplate: a review. *Terra Nova, 13,* 122-128.
594 Merriman, R.J., Evans, J.A., Leveridge, B.E. (2000). Devonian and Carboniferous volcanic
595 rocks associatied with the passive margin sequences of SW England; some geological
596 perspectives. *Proceedings of the Ussher Society, 10,* 77-85.
597 Miller, C.F., McDowell, S.M., Mapes, R.W. (2003). Hot and cold granites? Implications of
598 zircon saturation temperatures and preservation of inheritance. *Geology, 31*, 529-532.
599 Moore, J.M. (1975). A mechanical interpretation of the vein and dyke systems of the SW
600 England orefield. *Mineralium Deposita, 10*, 374-388.
601 Nance, R., Gutierrez-Alonso, G., Keppie, J., Linnemann, U., Murphy, J., Quesada, C. Strachan,
602 R.A., Woodcock, N.H. (2010). Evolution of the Rheic Ocean. *Gondwana Research, 17*,
603 194-222.
604 Nance, R.D., Neace, E.R., Braid, J.A., Murphy, J.B., Dupuis, N., Shail, R.K. (2015). Does the
605 Meguma terrane extend into SW England? *Geoscience Canada, 41*, 61-76.
606 http://dx.doi.org/10.12789/geocanj.2014.41.056
607 Penhallurick, R.D. (1986). Tin in antiquity: its mining and trade throughout the ancient world
608 with particular reference to Cornwall. *Institute of Metals,* London, 271 p.
609 Pownall, J.M., Waters, D.J., Searle, M.P., Robb, L.J., Shail, R.K. (2012). Shallow laccolithic
610 emplacement of the Land's End and Tregonning granites, Cornwall, UK: evidence from
611 aureole field relations and P-T modeling of cordierite-anthophyllite hornfels. *Geosphere,*
612 *8*, 1467-1504.

613 Quesada, C. (1998). A reappraisal of the structure of the Spanish segment of the Iberian Pyrite
614 Belt. *Mineralium Deposita, 33*, 31-34.
615 Rubatto, D. (2002). Zircon trace element geochemistry: partitioning with garnet and the link
616 between U-Pb ages and metamorphism. *Chemical Geology, 184*, 123-138.
617 Sandeman, H.A.I., Clark, A.H., Scott, D.J., Malpas, J.G. (2000). The Kennack Gneiss of the
618 Lizard Peninsula, Cornwall, SW England: commingling and mixing of mafic and felsic
619 magmas accompanying Givetian continental incorporation of the Lizard ophiolite. *Journal*
620 *of the Geological Society, London, 157*, 1227-1242.
621 Schofield, D.I., Millar, I.L., Wilby, P.R., Evans, J.A. (2010). A new, high precision U–Pb date
622 from the oldest known rocks in southern Britain. *Geological Magazine, 147*, 145-150.
623 Shackleton, R.M., Ries, A.C., Coward, M.P. (1982). An interpretation of the Variscan structures
624 in SW England. *Journal of the Geological Society of London, 139,* 533-541.
625 Shail, R.K., Wilkinson, J.J. (1994). Late- to post-Variscan extensional tectonics in south
626 Cornwall. *Proceedings of the Ussher Society, 8*, 228-236.
627 Shail, R.K., Alexander, A.C. (1997). Late Carboniferous to Triassic reactivation of Variscan
628 basement in the western English Channel: evidence from onshore exposures in south
629 Cornwall. *Journal of the Geological Society of London, 154*, 163-168.
630 Shail, R.K., Stuart, F.M., Wilkinson, J.J., Boyce, A.J. (2003). The role of post-Variscan
631 extensional tectonics and mantle melting in the generation of Lower Permian granites and
632 the giant W-As-Sn-Cu-Zn-Pb orefield of SW England. *Applied Earth Science;*
633 *Transactions of the Institutions of Mining and Metallurgy: Section B, 112*, 127-129.

634 Shail, R., Leveridge, B. (2009). The Rhenohercnian passive margin of SW England:
635 development, inversion and extensional reactivation. *Comptes Rendus Geoscience , 341*,
636 140-155.
637 Sláma, J., Košler, J., Condon, D.J., Crowley, J.L., Gerdes, A., Hanchar, J.M., Horstwood,
638 M.S.A., Morris, G.A., Nasdala, L., Norberg, N., Schaltegger, U., Schoene, B., Tubrett,
639 M.N., Whitehouse, M.J. (2008). Plešlovice zircon – a new natural reference material for
640 U–Pb and Hf isotopic microanalysis. *Chemical Geology 249*, 1-35.
641 Stimac, J.A., Clark, A.H., Chen, Y., Garcia, S. (1995). Enclaves and their bearing on the origin
642 of the Cornubian batholith, southwest England, *Mineralogical Magazine, 59*, 273–296.
643 Stone, M. (1995). The main Dartmoor granites: Petrogenesis and comparisons with the
644 Carnmenellis and Isles of Scilly granites. *Proceedings of the Ussher Society, 8*, 379-384.
645 Stone, M. (1997). A geochemical dichotomy in the Cornubian batholith. *Proceedings of the*
646 *Ussher Society, 9*, 206-210.
647 Stone, M. (2000)a. The early Cornubian plutons: a geochemical study, comparisons and some
648 implications. *Geosience in south-west England*, 10, 37-41.
649 Stone, M. (2000)b. Petrogenetic implications from biotite compositional variations in the
650 Cornubian granite batholith. *Mineralogical Magazine*, 64, 729-735.
651 Strachan, R.A., Linneman, U., Jeffries, T., Drost, K., Ulrich, J. (2014). Armorican provenance
652 for the mélange deposits below the Lizard ophiolite (Cornwall, UK): evidence for
653 Devonian obduction of Cadomian and Lower Paleozoic crust onto the southern margin of
654 Avalonia. *International Journal of Earth Sciences, 103,* 1359-1383.
655 Taylor, G.K. (2007). Pluton shapes in the Cornubian Batholith: new perspectives from gravity
656 modelling. *Journal of the Geological Society of London, 164,* 1-4.

Thorpe, R.S. (1987). Permian K-rich volcanic rocks of Devon: petrogenesis, tectonic setting and geological significance. *Transactions of the Royal Society of Edinburgh: Earth Sciences, 77,* 361-366.

von Raumer, J.F., Stampfli, G.M., Bussey, F. (2003). Gondwana-derived microcontinents – the constituents of the Variscan Alpine collisional orogens. *Tectonophysics 365*, 7-22. http://dx.doi.org/10.1016/S0040-1951(03)00015-5

Wan, Y., Liu, D., Dong, C., Liu, S., Wang, S., Yang, E. (2011). U-Th-Pb behavior of zircons under high-grade metamorphic conditions: a case study of zircon dating of metadiorite near Qixia, eastern Shandong. *Geoscience Frontiers, 2*, 137-146.

Watson, E.B., Harrison, T.M. (1983). Zircon saturation revisited: temperature and composition effects in a variety of crustal magma types. *Earth and Planetary Science Letters, 64*, 295-304.

Williamson, B.J., Müller, A., Shail, R.K. (2010). Source and partitioning of B and Sn in the Cornubian batholith of southwest England. *Ore Geology Reviews, 38,* 1-8.

Willis-Richards, J., Jackson, N.J. (1989). Evolution of the Cornubian ore field, southwest England: Part I. Batholith Modelling and Ore distribution. *Economic Geology, 84,* 1078-1100.

Zeh, A., Brätz, H., Miller, I., Williams, I. (2001). A combined zircon SHRIMP study of high-grade paragneisses from the Mid-German Crystalline Rise: evidence for northern Gondwanan and Grenvillian provenance. *Journal of the Geological Society, London*, *158*, 983-994.

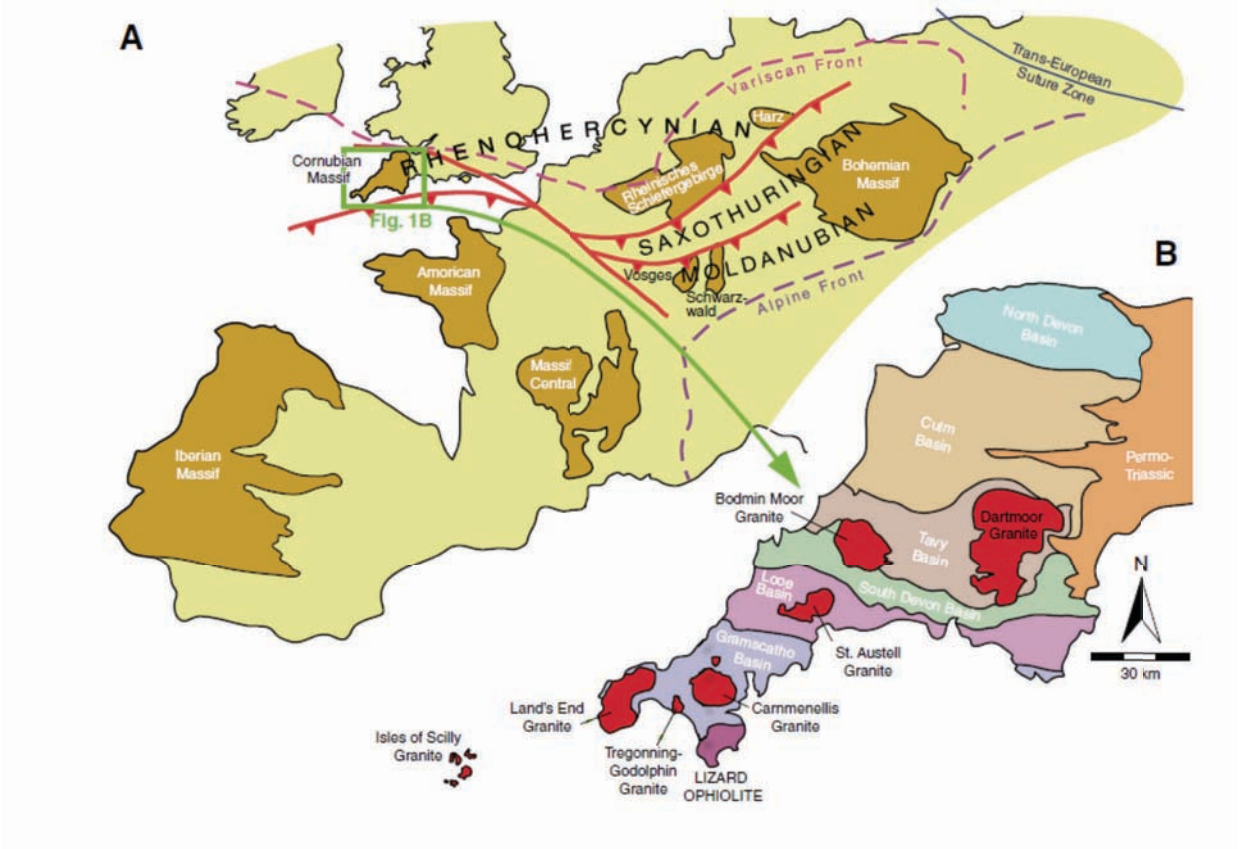

Figure 1: Modified from Pownall et al. (2012). Geological setting of the Cornubian granites within the European Variscides. (A) The Variscan belt of Europe during the Early Carboniferous, modified from Matte (1986) and Franke (1989). (B) Map of the Cornubian granites in the Western Rhenohercynian of SW England, after Shail and Leveridge (2009).

683

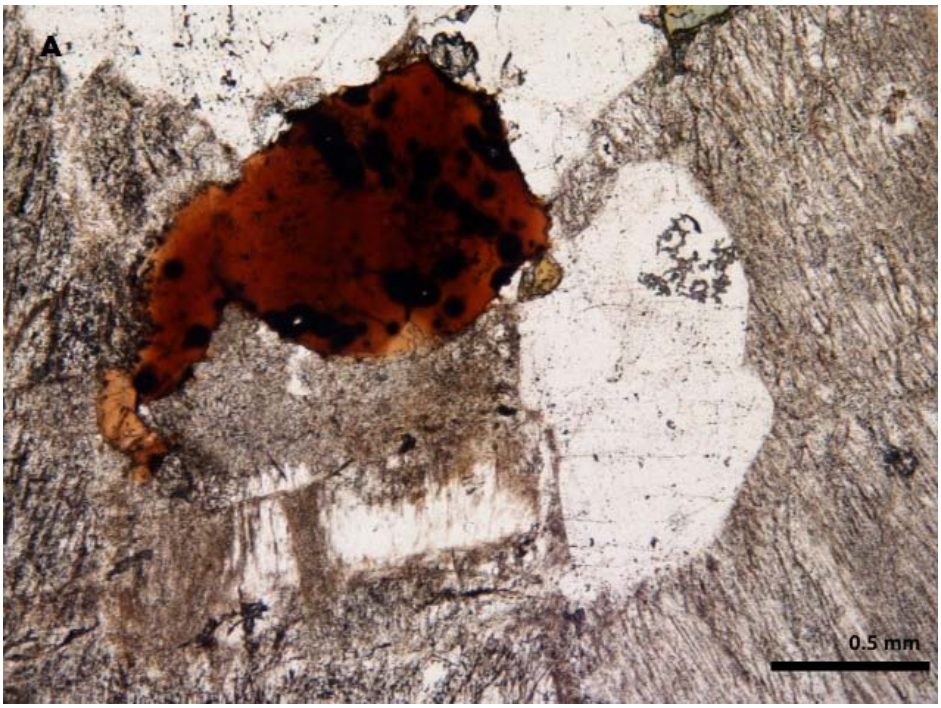

684

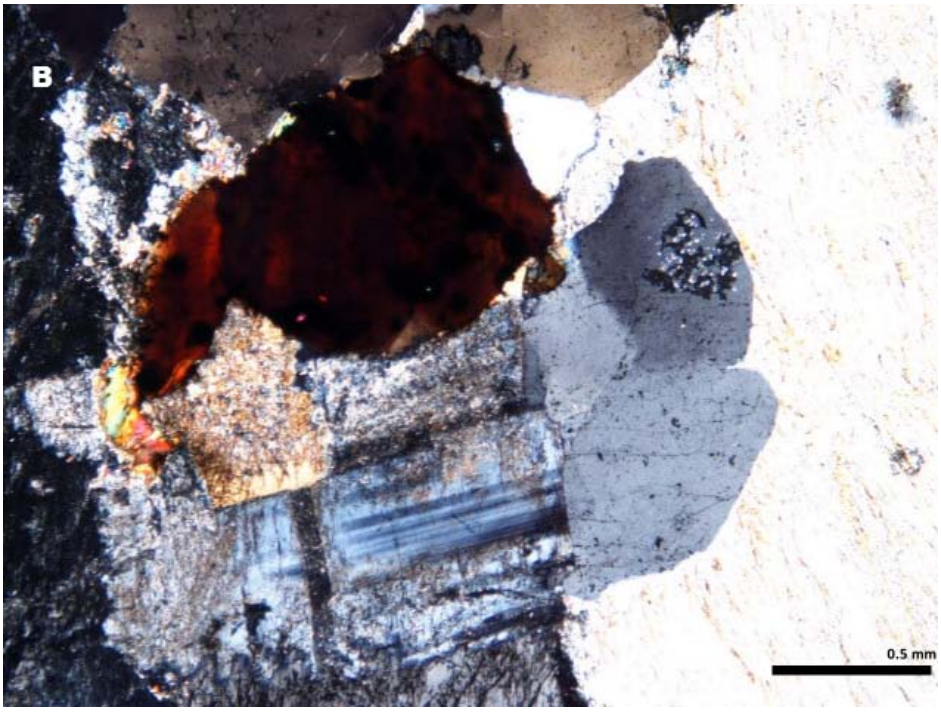

685

686 **Figure 2**: Thin section photos of the Dartmoor granite at 4x magnitude. Notice the dark areas of

687 radiation damage within the biotite. A) Plane-polarized light. B) Cross-polarized light.

Figure 3: SEM images of typical igneous zircons from the Dartmoor granite of the Cornubian Batholith and resulting data. Ellipses indicate analytical locations and % disc indicates discordance at > 10%.

693

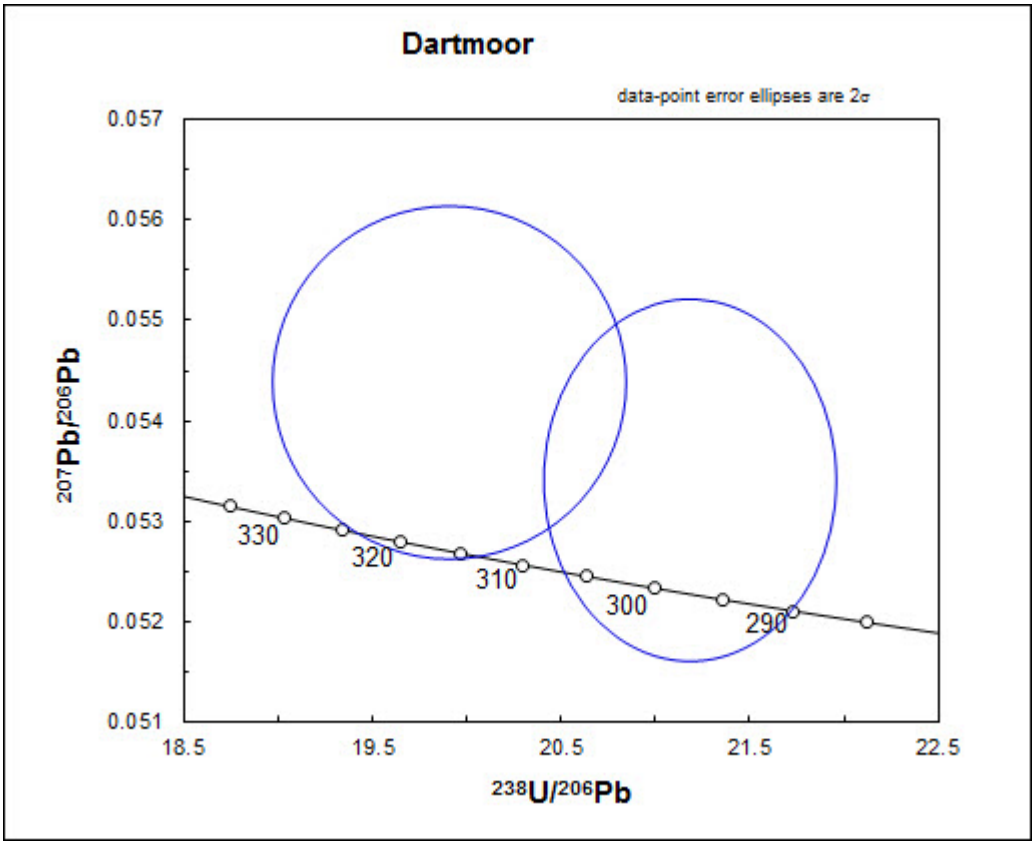

694

695 **Figure 4**: Tera Wasserburg plot of igneous zircon ages from the Dartmoor granite of the

696 Cornubian Batholith.

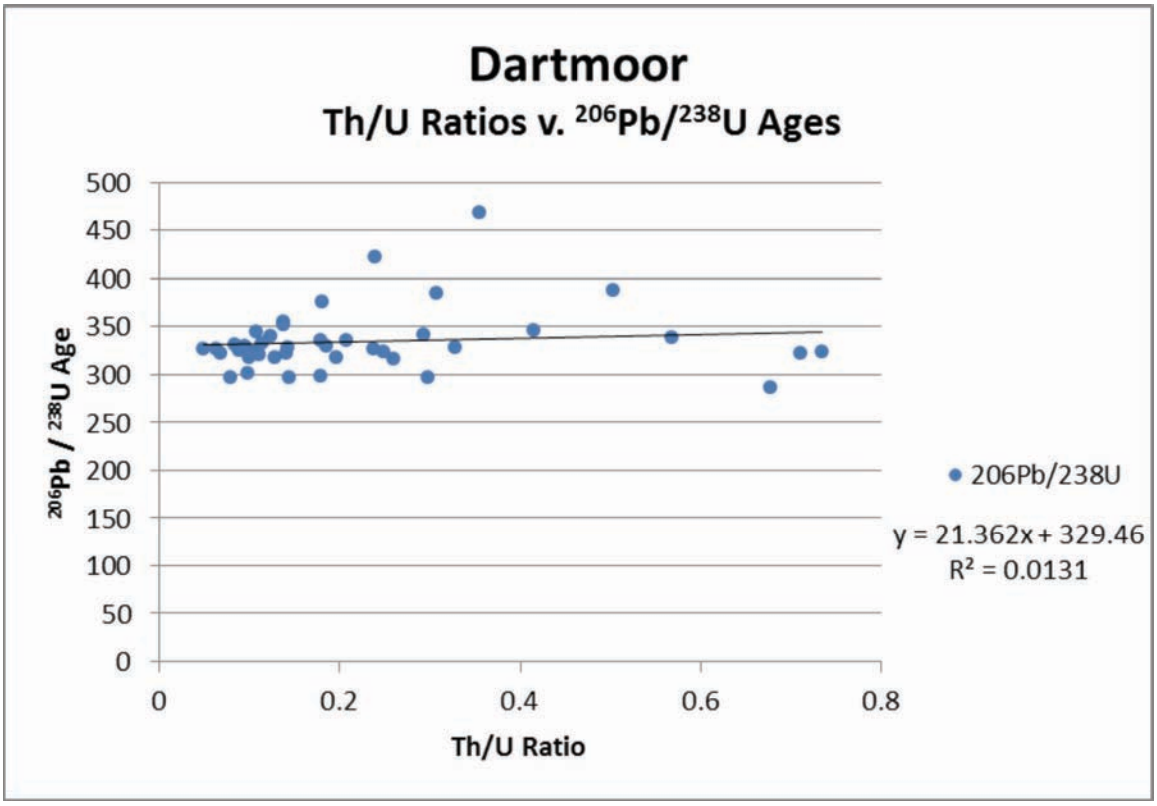

Figure 5: Scatter plot of Th/U ratios vs. $^{206}Pb/^{238}U$ Ages for the Dartmoor granite.

Figure 6: Thin section photos of the Bodmin Moor granite at 4x magnitude. Note the dark area of radiation damage within the biotite at the top of the pictures. A) Plane-polarized light. B) Cross-polarized light.

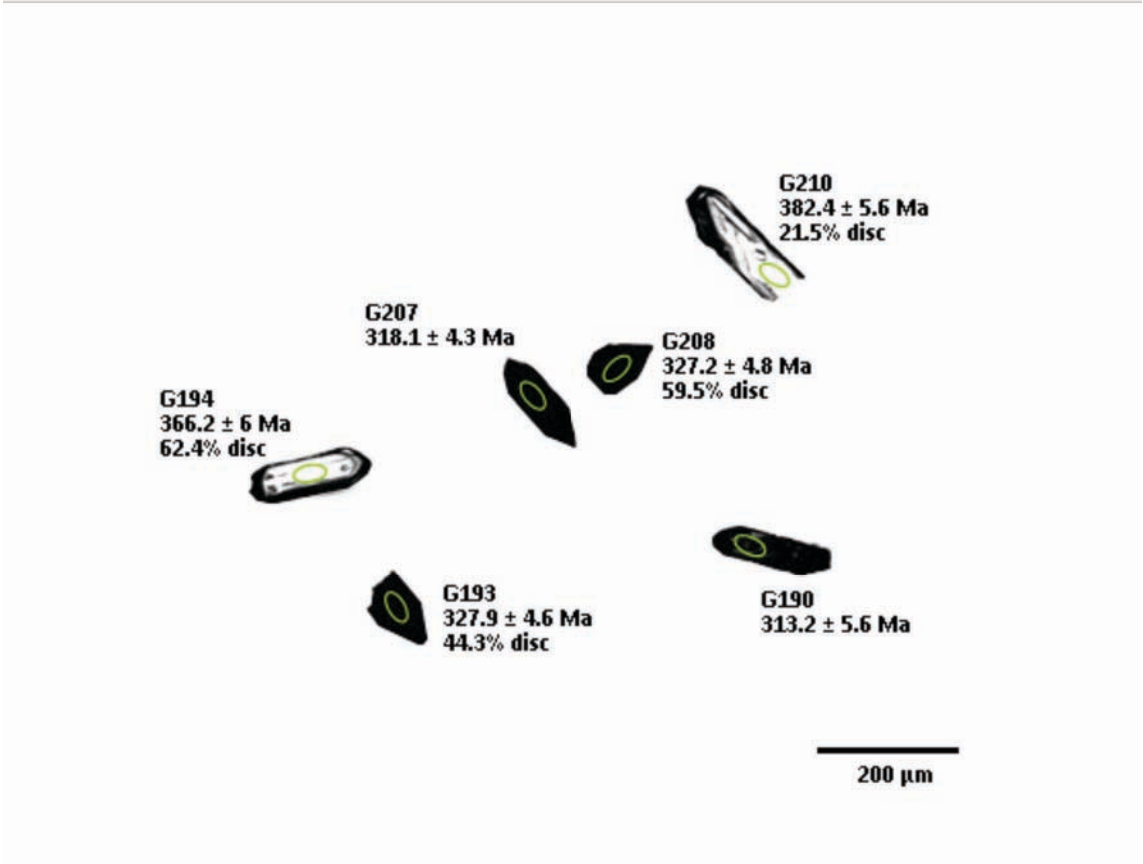

Figure 7: SEM images of typical igneous zircons from the Bodmin Moor granite of the Cornubian Batholith and resulting data. Ellipses indicate analytical locations and % disc indicates discordance at > 10%.

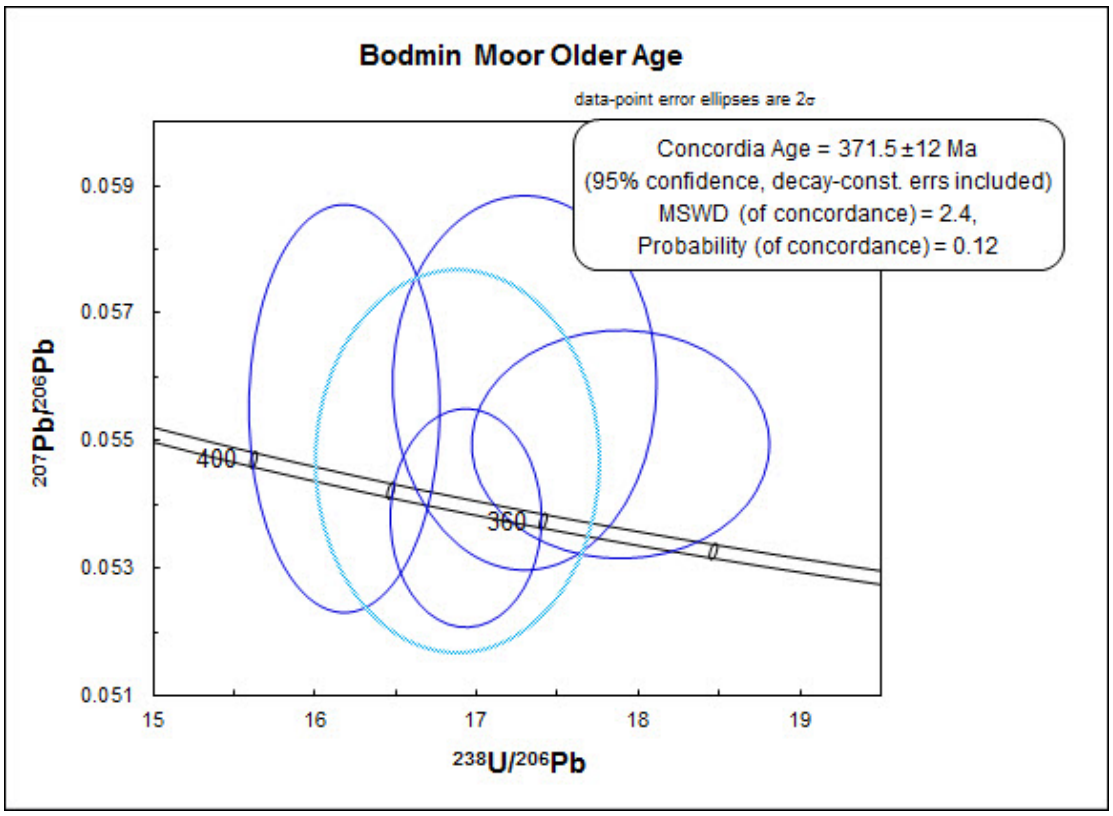

Figure 8: Tera Wasserburg plot of the older (inherited) igneous zircon ages from the Bodmin Moor granite of the Cornubian Batholith.

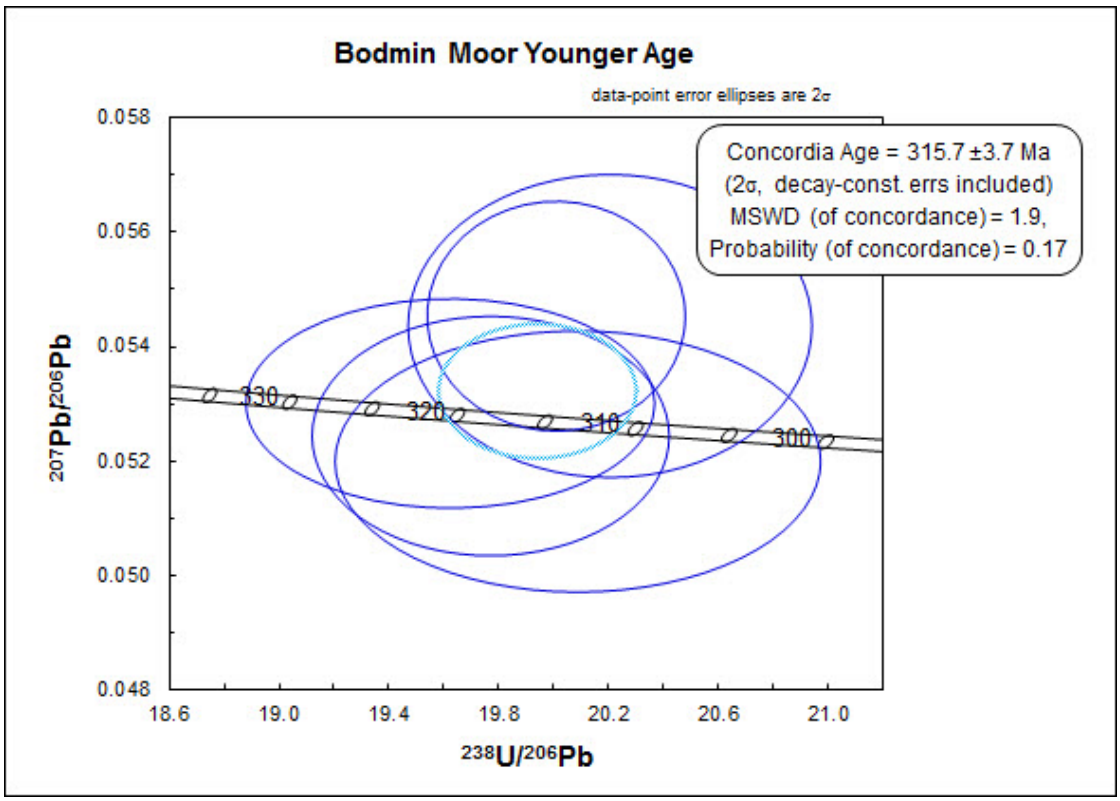

Figure 9: Tera Wasserburg plot of the younger igneous zircon ages from the Bodmin Moor granite of the Cornubian Batholith.

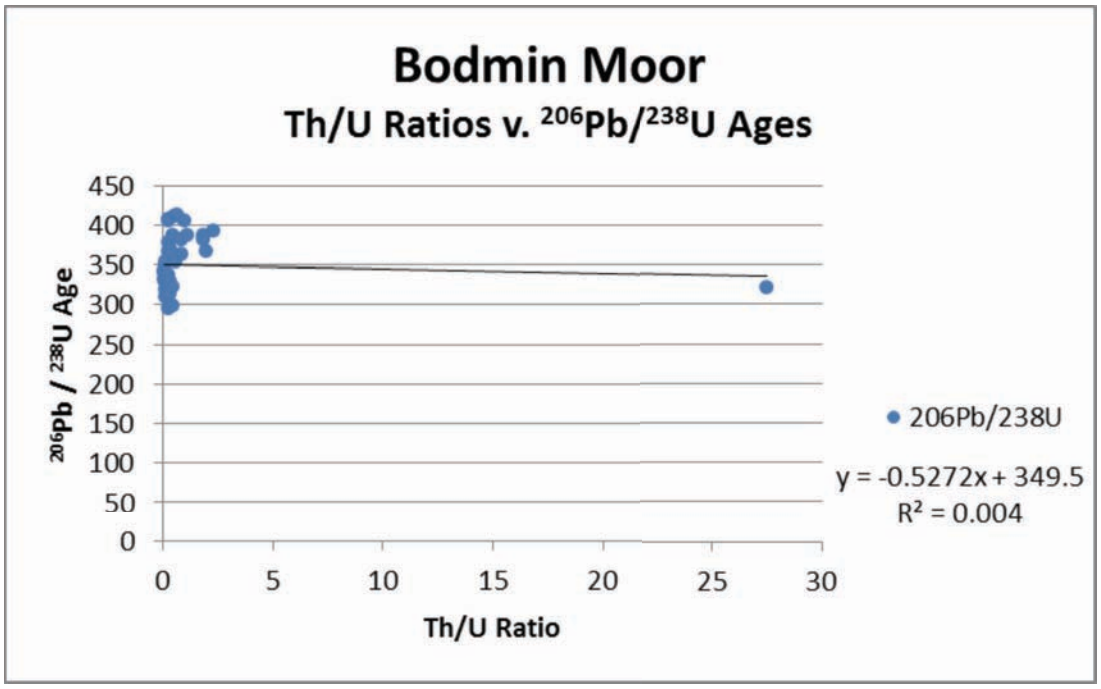

Figure 10: Scatter plot of Th/U ratios vs. $^{206}Pb/^{238}U$ Ages for the Bodmin Moor granite.

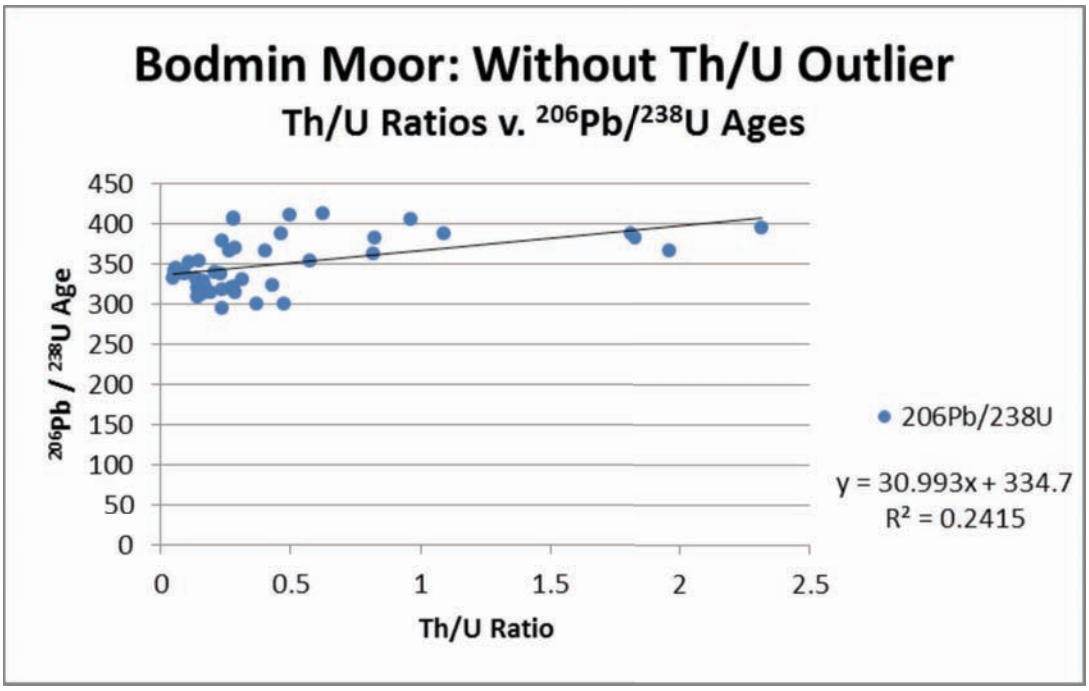

Figure 11: Scatter plot of Th/U ratios vs. $^{206}Pb/^{238}U$ Ages for the Bodmin Moor granite, excluding an extreme Th/U outlier.

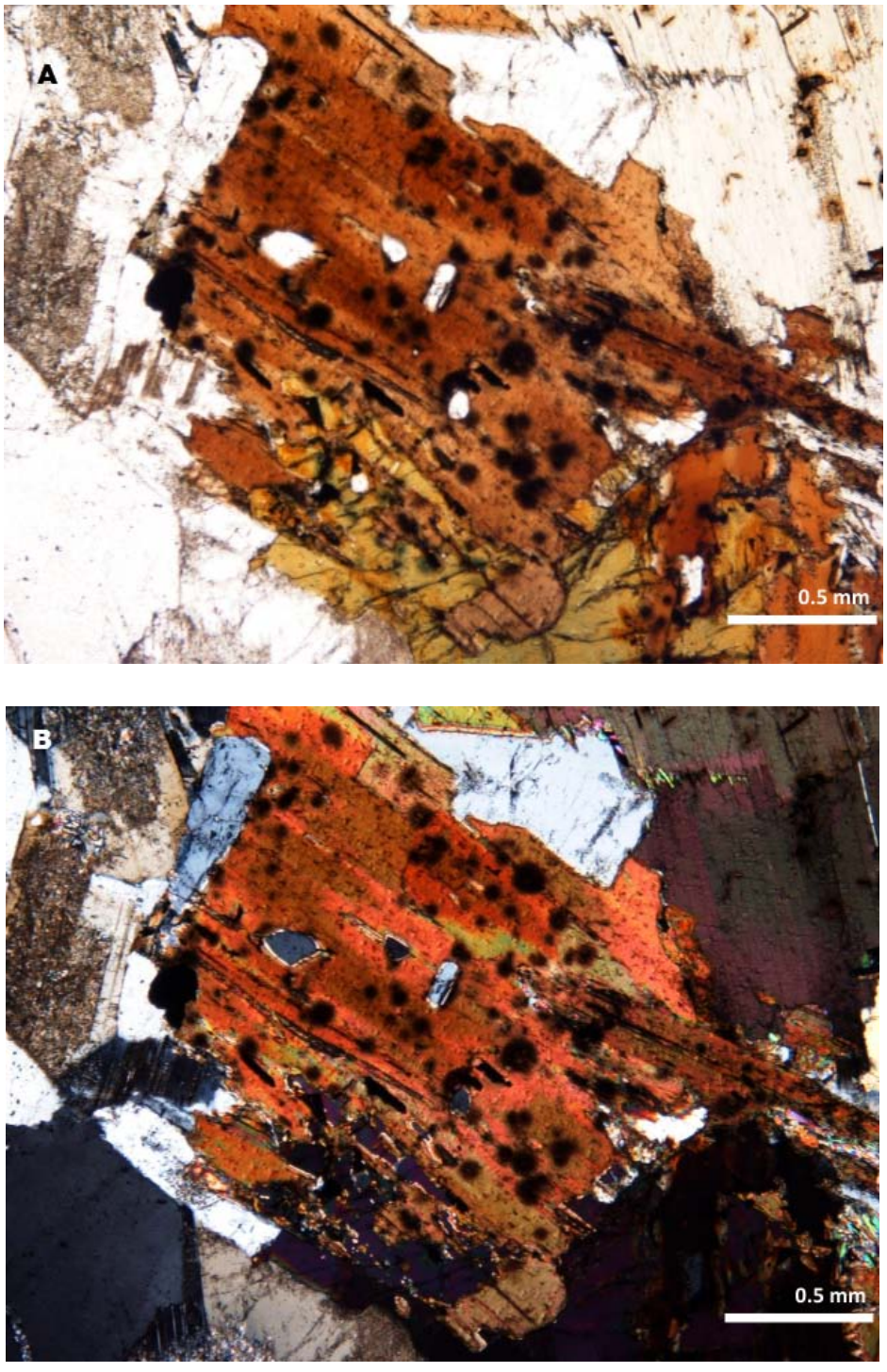

Figure 12: Thin section photos of the St Austell granite at 4x magnitude. Notice the dark areas of radiation damage within the biotite. A) Plane-polarized light. B) Cross-polarized light.

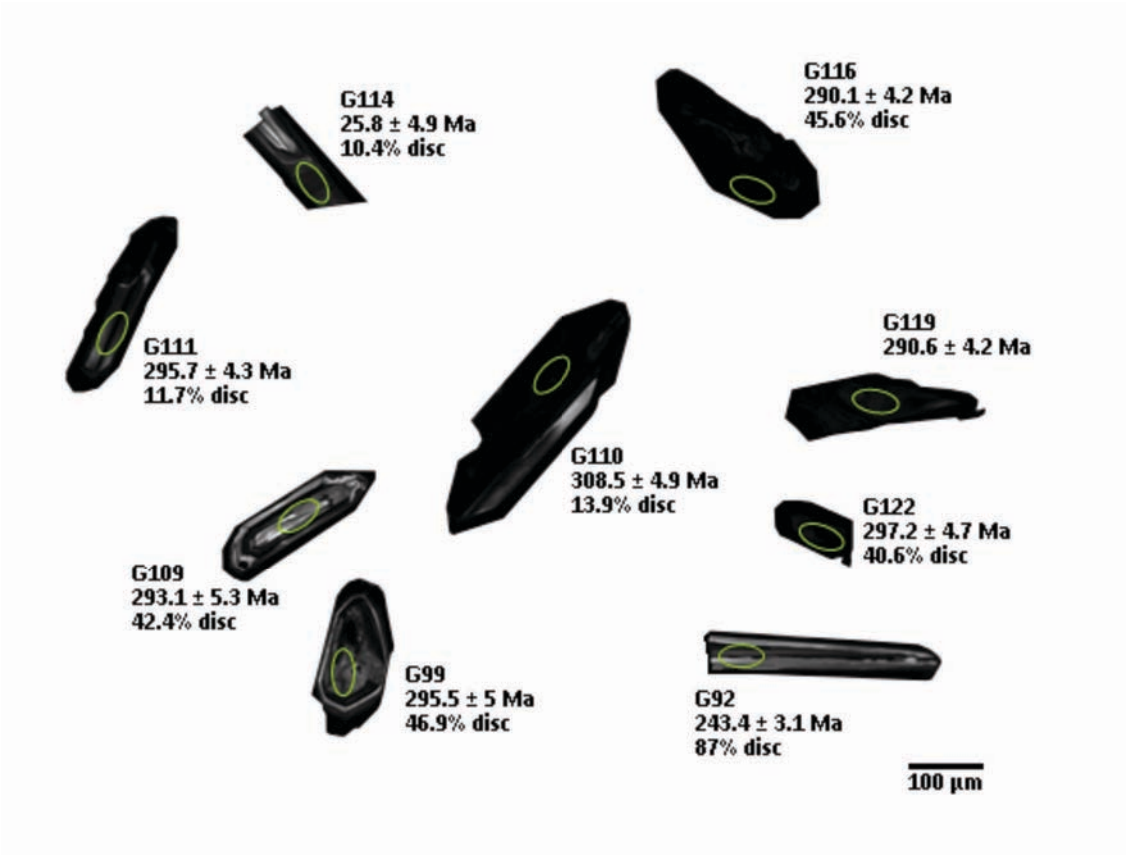

Figure 13: SEM images of typical igneous zircons from the St Austell granite of the Cornubian Batholith and resulting data. Ellipses indicate analytical locations and % disc indicates discordance at > 10%.

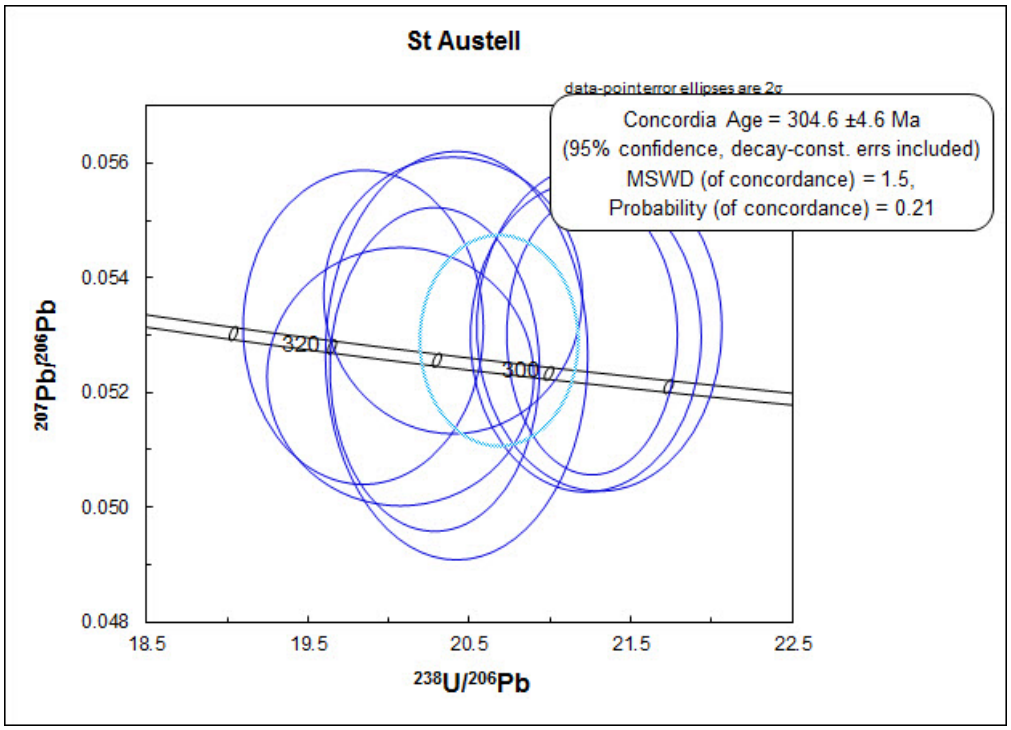

735

736 **Figure 14**: Tera Wasserburg plot of igneous zircon ages from the St Austell granite of the

737 Cornubian Batholith.

738

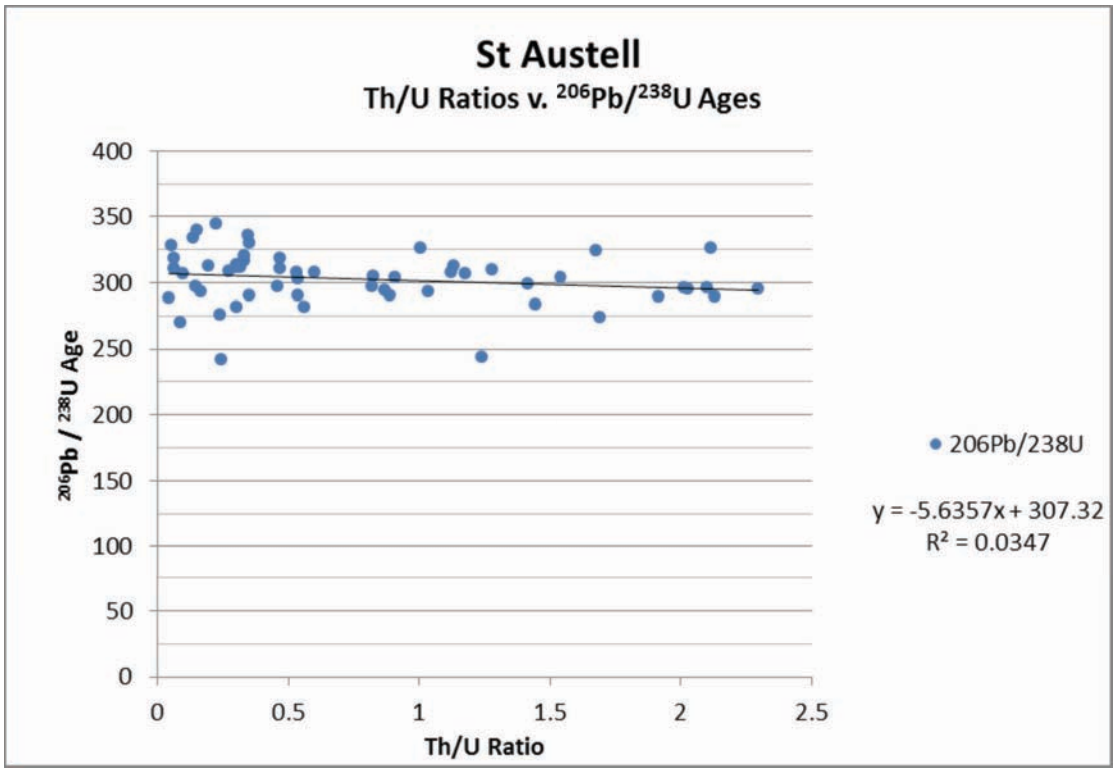

Figure 15: Scatter plot of Th/U ratios vs. $^{206}Pb/^{238}U$ Ages for the St Austell granite.

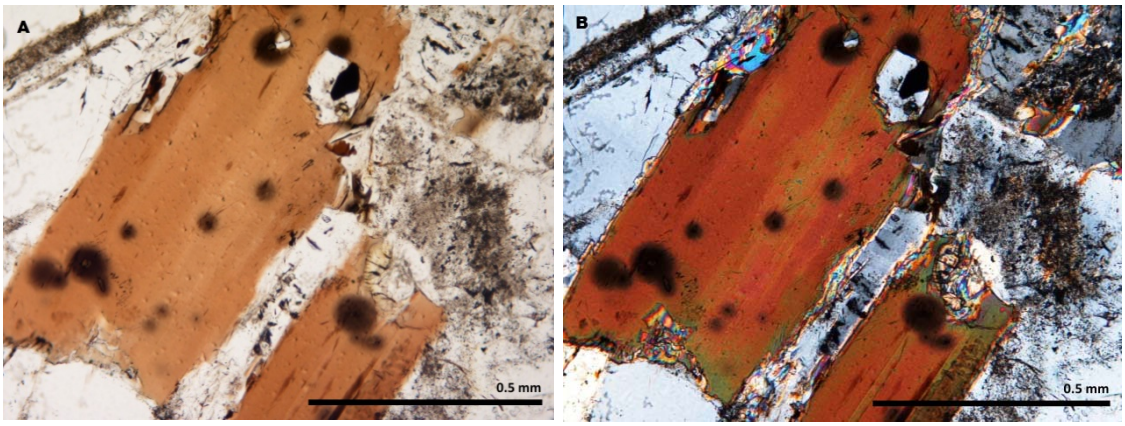

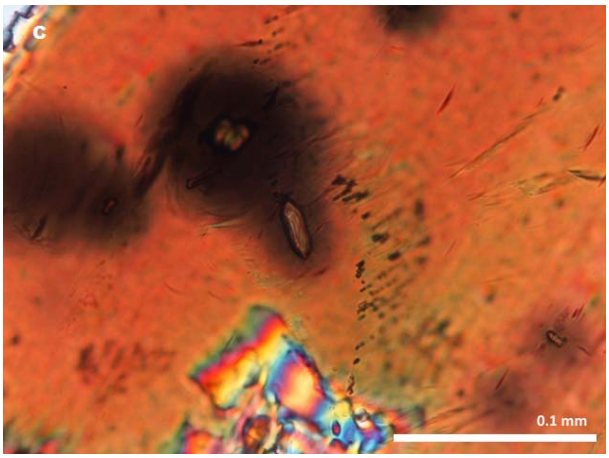

Figure 16: Thin section photos of the Carnmenellis granite. Note the dark areas of radiation damage within the biotite. A) Plane-polarized light at 10x magnitude. B) Cross-polarized light at 10x magnitude. C) A zircon in cross-section, cross-polarized light at 40x magnitude.

Figure 17: SEM images of typical igneous zircons from the Carnmenellis granite of the Cornubian Batholith and resulting data. Ellipses indicate analytical locations and % disc indicates discordance at > 10%.

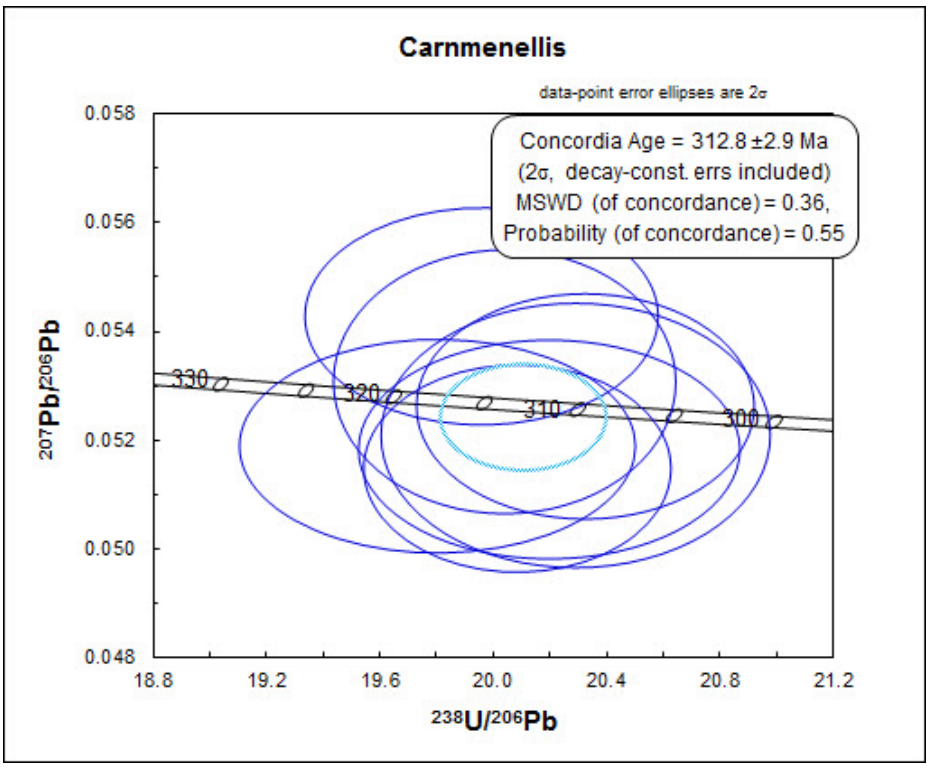

Figure 18: Tera Wasserburg plot of igneous zircon ages from the Carnmenellis granite of the Cornubian Batholith.

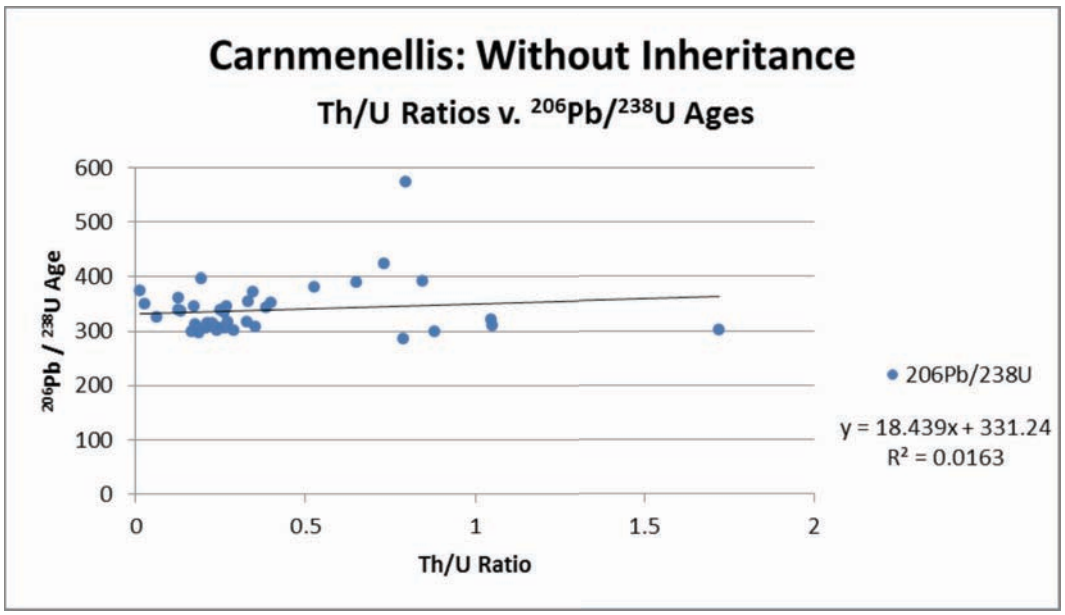

Figure 19: Scatter plot of Th/U ratios vs. $^{206}Pb/^{238}U$ Ages for the Carnmenellis granite.

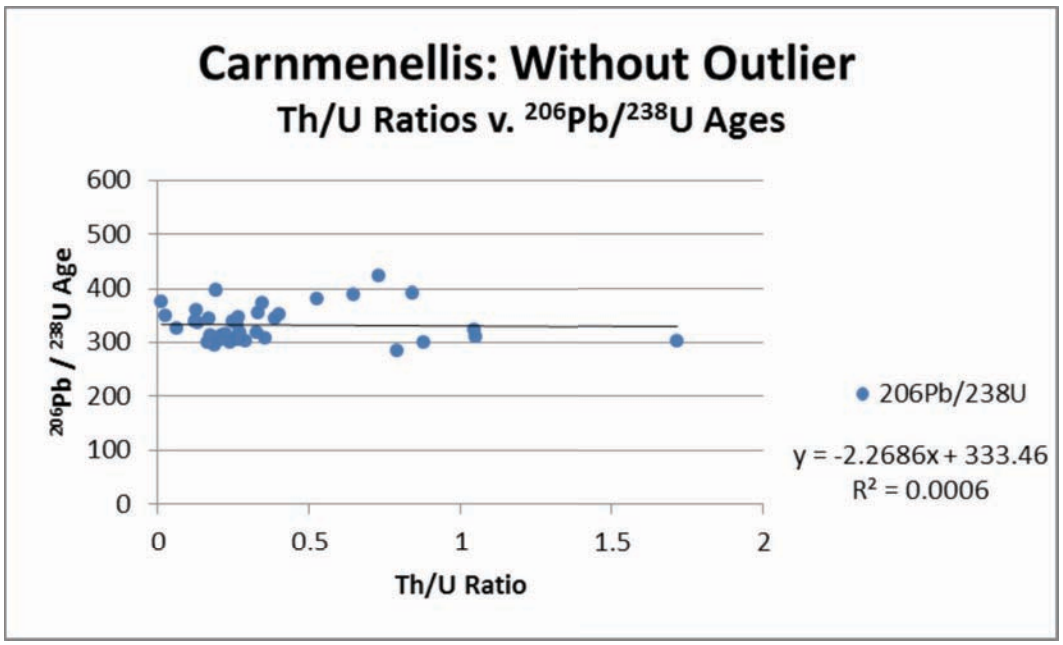

Figure 20: Scatter plot of Th/U ratios vs. 206Pb/238U Ages for the Carnmenellis granite with inherited ages excluded.

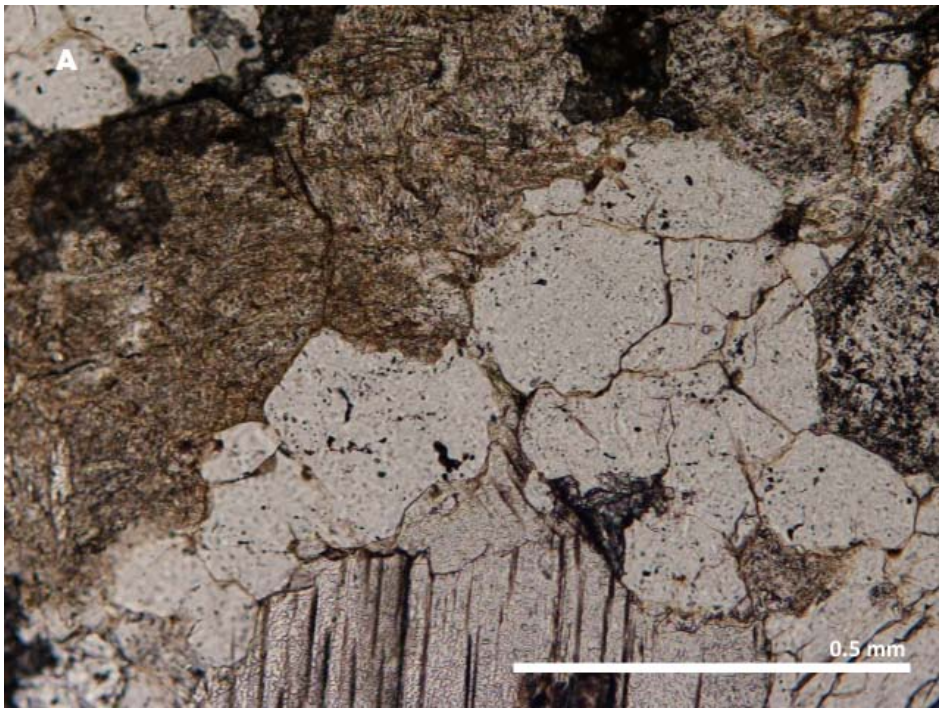

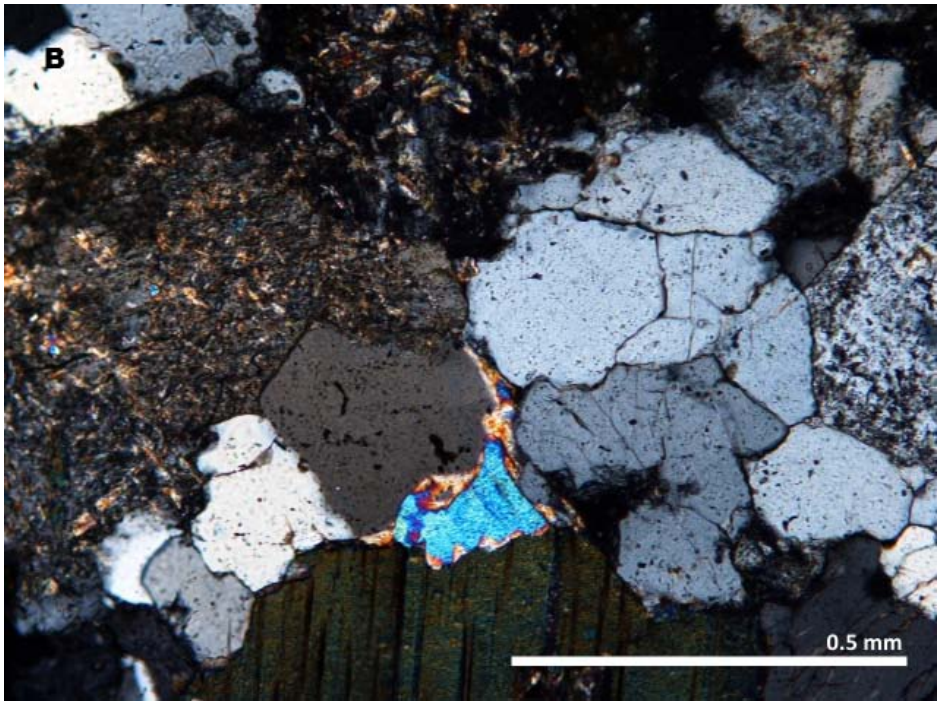

Figure 21: Thin section photos of the Land's End granite at 10x magnitude. No halos of radiation damage or zircons were visible, represented by the halo-free biotite in the bottom center. A) Plane-polarized light. B) Cross-polarized light.

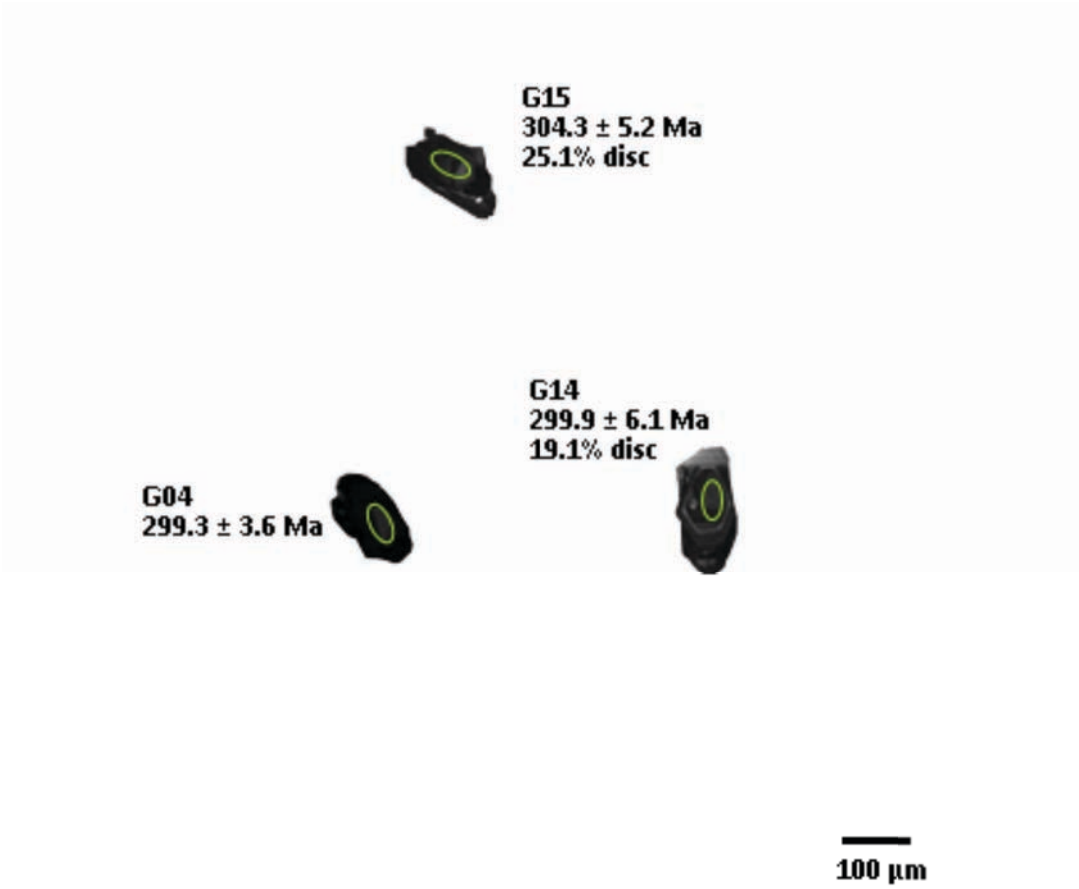

Figure 22: SEM images of typical igneous zircons from the Land's End granite of the Cornubian Batholith and resulting data. Ellipses indicate analytical locations and % disc indicates discordance at > 10%.

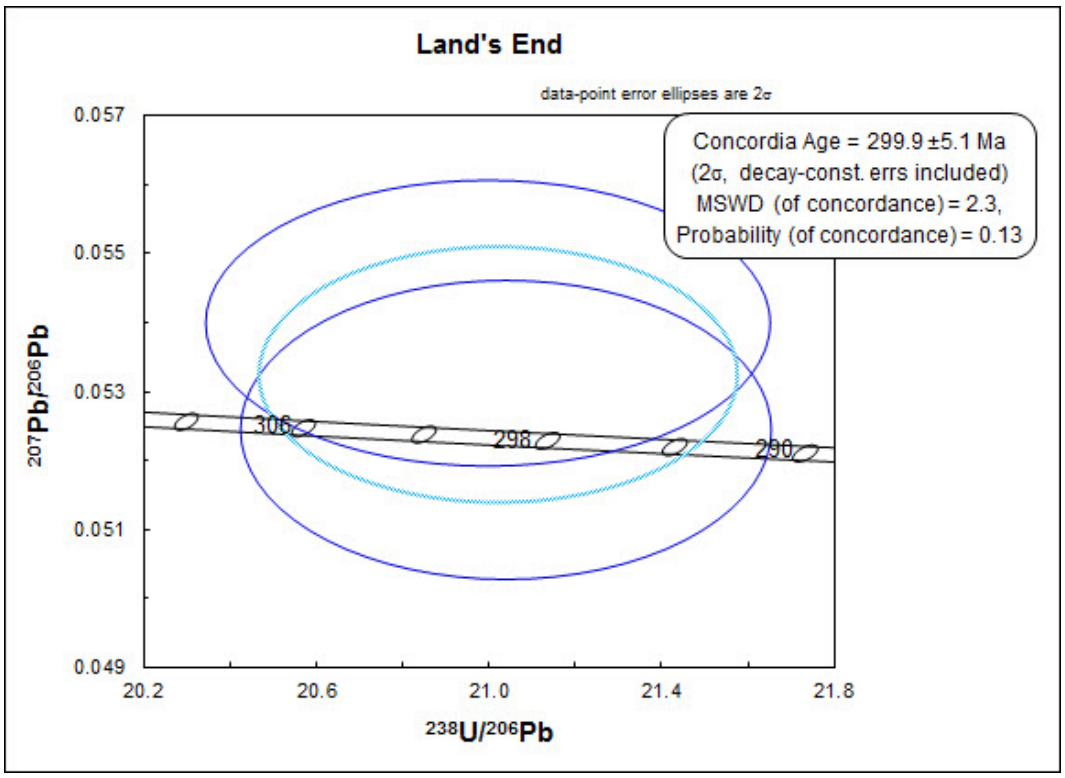

Figure 23: Tera Wasserburg plot of igneous zircon ages from the Land's End granite of the Cornubian Batholith.

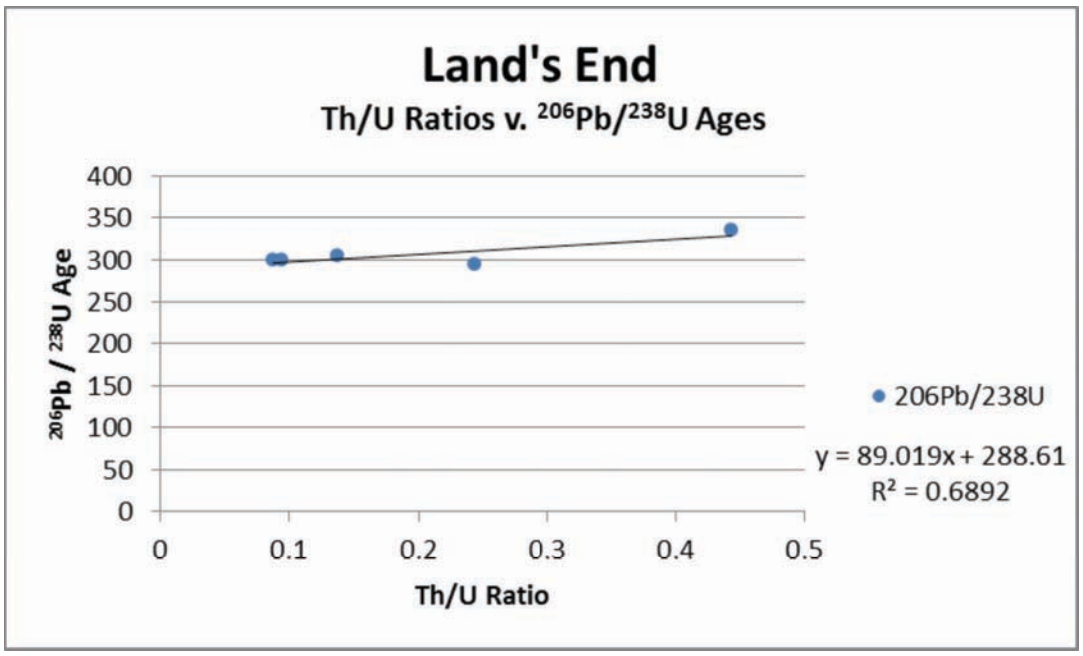

Figure 24: Scatter plot of Th/U ratios vs. 206Pb/238U Ages for the Land's End granite.

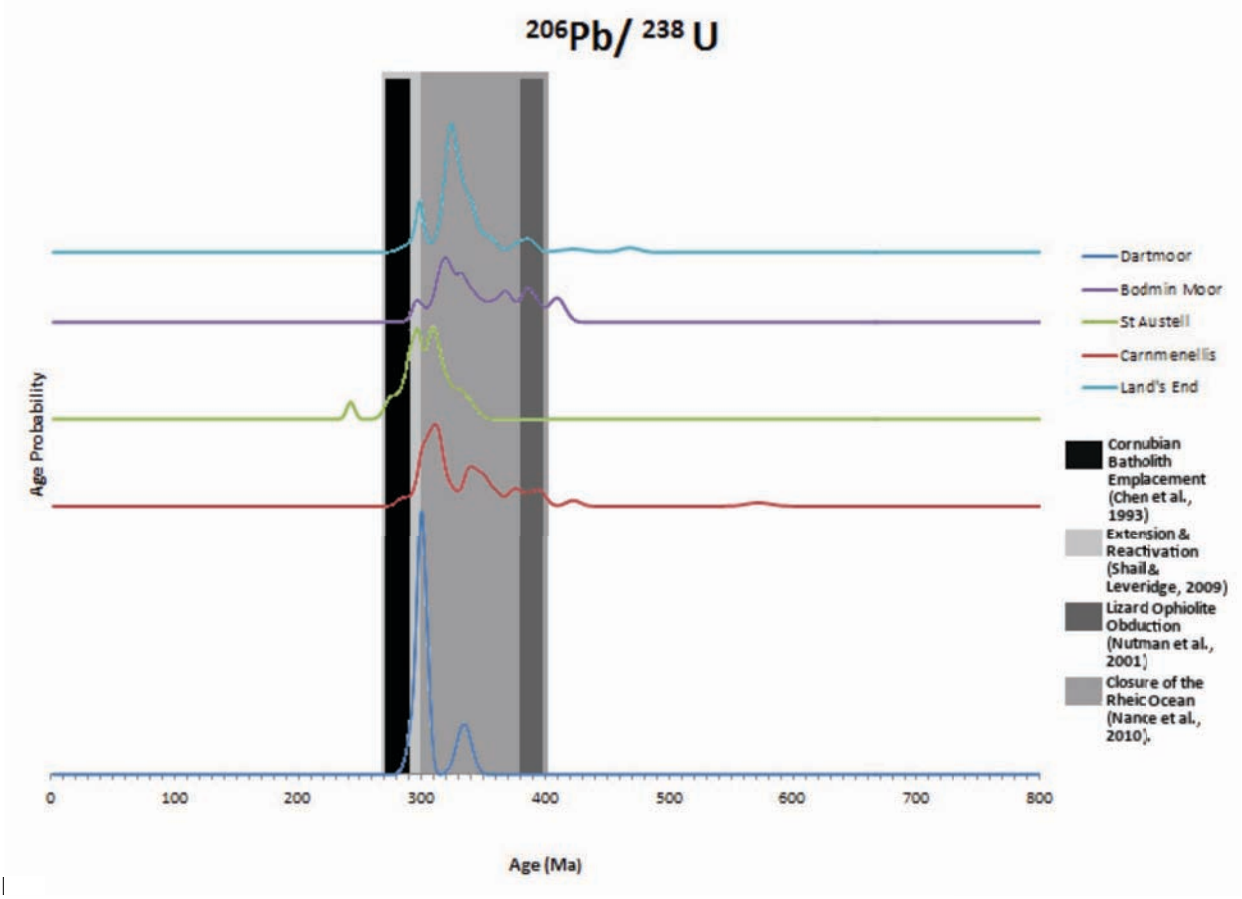

Figure 25: Age distribution plot for each of the five major plutons of the Cornubian Batholith shown in relations to the major tectonic and structural events related to its emplacement.

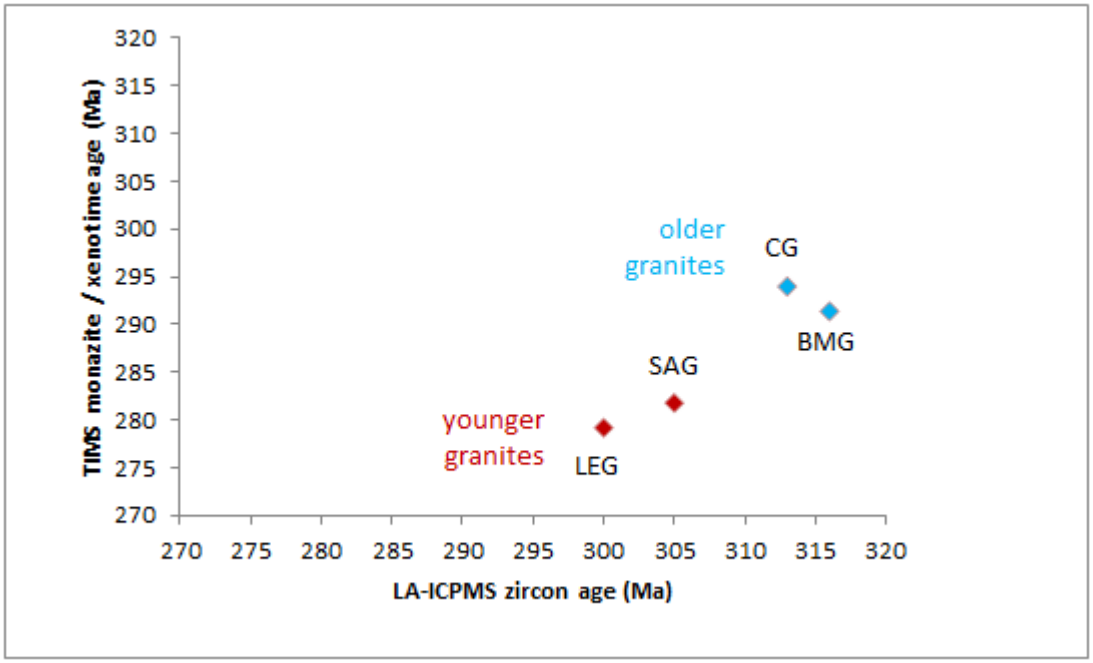

Figure 26: Comparison of LA-ICPMS U–Pb zircon ages (this study) with those from TIMS U–Pb monazite / xenotime (Chesley et al., 1993; Chen et al., 1993).

790

Dartmoor																					
	Concentrations				Ratios								Ages								
Samples	U (ppm)	Pb (ppm)	Th (ppm)	Th/U	$^{207}Pb/^{206}Pb$	1σ	$^{206}Pb/^{238}U$	1σ	$^{207}Pb/^{235}U$	1σ	$^{208}Pb/^{232}Th$	1σ	$^{207}Pb/^{206}Pb$	1σ Ma	$^{206}Pb/^{238}U$	1σ Ma	$^{207}Pb/^{235}U$	1σ Ma	$^{208}Pb/^{232}Th$	1σ Ma	Disc. %
DM G1.2	6880	304	678	0.1	0.0588	0.0011	0.048	0.001	0.358	0.010	0.021	0.001	560.8	10.9	301.3	6.9	310.6	8.3	419.5	23.8	46.3
DM G4.2	2755	157	379	0.1	0.0794	0.0017	0.056	0.001	0.557	0.016	0.049	0.003	1182.4	25.9	352.4	7.5	449.3	12.6	964.9	57.9	70.2
DM G5.1	1560	133	372	0.2	0.2360	0.0090	0.068	0.002	2.254	0.123	0.130	0.008	3093.3	117.6	422.7	11.3	1198.1	65.2	2475.3	153.7	86.3
DM G8.1	3830	198	707	0.2	0.0710	0.0017	0.053	0.001	0.474	0.014	0.035	0.002	956.0	23.2	330.3	7.1	393.8	11.7	699.6	42.0	65.5
DM G12.1	1017	44	81	0.1	0.0534	0.0007	0.047	0.001	0.320	0.005	0.014	0.001	346.2	4.8	297.3	4.4	281.8	4.4	286.1	15.5	14.1
DM G12.2	958	45	106	0.1	0.0545	0.0006	0.051	0.001	0.356	0.005	0.019	0.001	390.1	4.5	321.3	3.6	309.0	4.2	387.6	19.4	17.6
DM G19.1	2047	101	100	0.0	0.0828	0.0014	0.052	0.001	0.565	0.012	0.140	0.008	1263.7	20.7	326.5	4.0	454.7	9.5	2655.7	144.1	74.2
DM G97.2	1104	54	111	0.1	0.0694	0.0008	0.051	0.001	0.454	0.006	0.048	0.002	909.6	11.0	322.7	3.6	380.1	5.3	953.3	45.6	64.5
DM G108.1	348	15	50	0.1	0.0566	0.0008	0.047	0.001	0.356	0.007	0.021	0.001	475.1	6.8	297.0	3.2	309.6	5.8	413.5	23.0	37.5
DM G109.1	541	36	97	0.2	0.1196	0.0025	0.060	0.001	0.936	0.026	0.113	0.005	1950.8	40.4	375.7	5.7	670.8	18.4	2167.4	101.8	80.7
DM G113.1	447	31	61	0.1	0.1403	0.0033	0.057	0.001	1.051	0.030	0.162	0.008	2231.4	52.8	355.6	5.0	729.4	20.9	3029.3	154.9	84.1
DM G116.1	422	52	150	0.4	0.2600	0.0047	0.075	0.001	2.576	0.074	0.190	0.009	3246.7	58.6	468.5	8.3	1293.7	37.1	3517.9	159.0	85.6
DM G121.1	309	28	156	0.5	0.2022	0.0046	0.062	0.001	1.722	0.055	0.115	0.008	2844.1	64.1	387.1	6.2	1016.7	32.8	2200.9	154.0	86.4
DM G122.1	827	38	149	0.2	0.0680	0.0009	0.047	0.000	0.415	0.007	0.028	0.001	868.8	11.2	298.8	3.0	352.5	5.6	567.5	24.0	65.6
DM G129.1	560	27	61	0.1	0.0657	0.0011	0.051	0.001	0.434	0.009	0.038	0.002	798.1	13.7	323.5	3.3	365.7	7.5	758.5	40.5	59.5
DM G225.1	739	42	84	0.1	0.1036	0.0016	0.053	0.001	0.710	0.013	0.109	0.005	1689.0	25.5	333.0	4.1	544.7	10.2	2095.6	94.0	80.3
DM G226.2	615	31	121	0.2	0.0746	0.0011	0.050	0.001	0.484	0.008	0.034	0.002	1058.0	15.2	317.3	4.0	401.0	6.5	671.1	32.1	70.0
DM G229.1	207	13	118	0.6	0.1321	0.0026	0.054	0.001	0.972	0.025	0.043	0.002	2125.6	41.5	338.1	4.0	689.6	17.5	848.5	38.5	84.1
DM G230.1	503	27	120	0.2	0.0830	0.0016	0.052	0.001	0.557	0.012	0.045	0.002	1269.7	25.0	326.3	4.5	449.8	9.6	889.4	48.6	74.3
DM G260.1	390	40	120	0.3	0.2397	0.0061	0.062	0.001	1.969	0.058	0.161	0.009	3117.9	79.9	385.2	5.8	1105.0	32.7	3018.4	165.5	87.6
DM G313.1	473	25	118	0.2	0.0807	0.0014	0.051	0.001	0.534	0.013	0.037	0.002	1213.9	21.6	323.1	4.8	434.7	10.8	739.9	32.2	73.4
DM G318.1	632	37	78	0.1	0.1103	0.0022	0.054	0.001	0.755	0.018	0.111	0.005	1804.6	35.8	339.6	4.0	571.2	13.6	2127.9	92.4	81.2
DM G324.1	1269	62	106	0.1	0.0581	0.0008	0.053	0.001	0.374	0.007	0.027	0.001	531.9	7.5	330.7	4.8	322.4	5.9	536.2	22.4	37.8
DM G325.1	1417	70	134	0.1	0.0649	0.0010	0.052	0.001	0.418	0.008	0.041	0.002	771.4	11.7	329.2	4.4	354.9	6.6	811.3	38.1	57.3
DM G331.1	375	22	110	0.3	0.1035	0.0022	0.054	0.001	0.746	0.021	0.049	0.002	1688.2	36.5	341.9	4.2	566.0	15.6	961.8	44.7	79.7
DM G335.1	414	22	86	0.2	0.0755	0.0017	0.054	0.001	0.531	0.014	0.038	0.002	1081.0	24.0	336.2	5.9	432.6	11.8	746.4	41.3	68.9
DM G336.1	191	12	140	0.7	0.1305	0.0028	0.051	0.001	0.928	0.024	0.030	0.002	2105.1	45.1	323.1	4.3	666.7	17.0	605.5	44.2	84.7
DM G337.1	652	40	116	0.2	0.1190	0.0025	0.053	0.001	0.813	0.020	0.090	0.007	1941.7	41.3	335.4	4.3	603.9	15.1	1739.9	132.1	82.7
DM G338.1	571	29	80	0.1	0.0779	0.0017	0.051	0.001	0.508	0.012	0.046	0.004	1145.4	25.3	322.6	4.3	417.0	9.7	909.7	71.8	71.8
DM G340.1	401	22	51	0.1	0.1066	0.0028	0.051	0.001	0.702	0.019	0.104	0.008	1742.6	45.2	318.0	4.2	539.9	14.8	2005.3	155.7	81.8
DM G343.1	725	36	72	0.1	0.0799	0.0018	0.050	0.001	0.519	0.013	0.061	0.005	1195.4	26.9	317.5	6.0	424.4	10.2	1195.0	90.7	73.4
DM G350.1	215	12	70	0.3	0.1143	0.0030	0.052	0.001	0.819	0.027	0.048	0.004	1869.2	49.3	327.5	5.4	607.5	20.2	956.6	70.4	82.5
DM G356.1	698	33	48	0.1	0.0568	0.0010	0.051	0.001	0.358	0.007	0.024	0.002	483.0	8.5	322.4	4.5	310.7	6.1	469.7	39.6	33.2
DM G357.1	588	30	83	0.1	0.0675	0.0013	0.052	0.001	0.450	0.010	0.036	0.003	853.9	16.0	327.8	5.0	377.1	8.4	712.2	56.7	61.6
DM G470.1	320	19	227	0.7	0.1141	0.0031	0.051	0.001	0.765	0.030	0.028	0.002	1866.0	51.3	322.1	7.4	577.1	22.5	565.1	45.2	82.7
DM G470a.1	269	12	80	0.3	0.0646	0.0013	0.047	0.001	0.415	0.015	0.021	0.002	761.1	15.4	297.1	6.0	352.3	12.7	413.1	33.7	61.0
DM G471.1	665	40	275	0.4	0.1009	0.0027	0.055	0.001	0.715	0.028	0.039	0.003	1641.4	44.0	346.0	6.7	547.8	21.3	772.0	64.3	78.9
DM G474.1	399	19	103	0.3	0.0544	0.0007	0.050	0.001	0.353	0.010	0.017	0.001	386.9	5.1	315.9	6.1	306.9	9.0	350.6	27.8	18.3
DM G479.1	720	40	77	0.1	0.0970	0.0024	0.055	0.001	0.677	0.027	0.116	0.012	1566.8	38.9	344.3	8.5	524.7	21.3	2216.4	233.8	78.0
DM G483.1	309	14	209	0.7	0.0582	0.0012	0.045	0.001	0.356	0.012	0.014	0.001	535.7	10.7	286.6	6.2	309.4	10.3	282.6	22.2	46.5
DM G483.2	1192	60	106	0.1	0.0760	0.0013	0.052	0.001	0.506	0.016	0.063	0.005	1095.2	18.5	325.7	6.0	415.5	13.0	1233.8	100.3	70.3
DM G485.2	1096	52	69	0.1	0.0550	0.0007	0.052	0.001	0.362	0.010	0.023	0.002	412.8	5.0	327.3	6.0	313.6	8.9	458.9	38.7	20.7

791

792 **Table 1**: Laser ablation ICPMS U–Pb-Th data and calculated ages for zircons from the

793 Dartmoor granite, Cornwall.

794

Bodmin Moor																					
	Concentrations				Ratios								Ages								
Samples	U (ppm)	Pb (ppm)	Th (ppm)	Th/U	$^{207}Pb/^{206}Pb$	1σ	$^{206}Pb/^{238}U$	1σ	$^{207}Pb/^{235}U$	1σ	$^{208}Pb/^{232}Th$	1σ	$^{207}Pb/^{206}Pb$	1σ Ma	$^{206}Pb/^{238}U$	1σ Ma	$^{207}Pb/^{235}U$	1σ Ma	$^{208}Pb/^{232}Th$	1σ Ma	Disc. %
BM sm G240.1	500	29	73	0.1	0.0989	0.0022	0.056	0.001	0.710	0.018	0.087	0.008	1603.1	35.5	353.6	6.2	544.7	13.9	1679.5	160.8	77.9
BM sm G245.1	740	36	101	0.1	0.0577	0.0009	0.053	0.001	0.385	0.008	0.019	0.002	517.1	7.8	331.7	5.3	330.8	6.9	371.2	35.0	35.9
BM sm G243.1	643	31	60	0.1	0.0532	0.0009	0.054	0.001	0.357	0.007	0.016	0.002	339.2	5.4	336.2	5.5	310.2	6.5	328.6	30.6	0.9
BM sm G235.1	393	20	91	0.2	0.0577	0.0010	0.054	0.001	0.407	0.010	0.019	0.002	517.8	9.4	336.9	5.5	346.5	8.8	389.0	38.3	34.9
BM sm G218.1	98	6	28	0.3	0.0542	0.0013	0.065	0.001	0.493	0.014	0.019	0.002	378.4	8.9	407.5	6.7	407.0	11.4	374.0	35.6	-7.7
BM sm G216.1	180	8	29	0.2	0.0544	0.0011	0.049	0.001	0.362	0.008	0.015	0.001	386.0	7.7	311.4	4.6	313.6	7.1	304.5	29.0	19.3
BM sm G211.1	905	42	129	0.1	0.0572	0.0009	0.051	0.001	0.366	0.008	0.021	0.001	501.0	7.8	318.4	4.9	316.5	6.9	426.5	20.1	36.4
BM sm G210.1	70	4	58	0.8	0.0569	0.0017	0.061	0.001	0.480	0.015	0.019	0.001	487.3	14.4	382.4	5.6	398.0	12.5	382.9	16.7	21.5
BM sm G207.1	356	17	84	0.2	0.0524	0.0009	0.051	0.001	0.347	0.007	0.015	0.001	304.5	5.0	318.1	4.3	302.4	5.9	293.3	13.0	-4.5
BM sm G208.1	612	31	100	0.2	0.0661	0.0012	0.052	0.001	0.438	0.010	0.030	0.001	808.4	14.2	327.2	4.8	369.0	8.3	594.2	26.8	59.5
BM sm G194.1	108	6	29	0.3	0.0715	0.0020	0.058	0.001	0.557	0.016	0.025	0.001	973.1	27.3	366.2	6.1	449.7	13.0	498.7	24.2	62.4
BM sm G193.1	720	35	105	0.1	0.0596	0.0011	0.052	0.001	0.396	0.010	0.023	0.001	589.0	10.6	327.9	4.6	338.5	8.1	456.1	25.7	44.3
BM sm G190.1	445	21	87	0.2	0.0520	0.0009	0.050	0.001	0.338	0.008	0.015	0.001	285.0	5.1	313.2	5.6	295.7	6.8	303.5	13.5	-9.9
BM sm G188.1	234	15	109	0.5	0.0657	0.0012	0.062	0.001	0.558	0.013	0.025	0.001	798.3	14.9	387.5	5.7	450.4	10.5	504.1	21.5	51.5
BM sm G178.1	397	24	94	0.2	0.0684	0.0012	0.060	0.001	0.557	0.015	0.034	0.002	880.3	15.9	378.1	7.0	449.5	12.0	684.6	41.1	57.0
BM sm G177.1	238	11	88	0.4	0.0527	0.0010	0.047	0.001	0.349	0.009	0.015	0.001	316.5	5.9	298.9	5.0	303.6	7.6	303.2	16.0	5.5
BM sm G183.1	258	12	123	0.5	0.0548	0.0009	0.048	0.001	0.349	0.008	0.017	0.001	402.4	6.7	299.2	4.8	304.3	6.6	332.5	19.7	25.6
BM sm G170.1	368	18	101	0.3	0.0514	0.0009	0.051	0.001	0.340	0.007	0.015	0.001	257.9	4.3	318.4	4.5	297.3	5.9	294.4	14.5	-23.5
BM sm G168.1	1375	66	71	0.1	0.0603	0.0008	0.054	0.001	0.414	0.009	0.029	0.002	615.7	8.3	341.0	6.1	351.7	7.3	579.9	31.9	44.6
BM sm G172.1	509	25	219	0.4	0.0519	0.0008	0.051	0.001	0.337	0.006	0.015	0.001	279.4	4.1	322.5	4.8	294.6	5.3	293.1	14.2	-15.4
BM sm G167.1	204	11	43	0.2	0.0618	0.0011	0.054	0.001	0.456	0.011	0.024	0.001	667.7	12.1	338.1	6.1	381.3	9.4	477.7	28.9	49.4
BM sm G152.1	35	3	64	1.8	0.0648	0.0025	0.061	0.001	0.607	0.039	0.017	0.001	768.3	29.1	382.3	7.0	481.9	31.1	350.0	18.4	50.2
BM sm G125.1	86	6	94	1.1	0.0555	0.0013	0.062	0.001	0.500	0.015	0.017	0.001	432.6	10.2	386.6	5.8	411.5	12.0	344.1	16.8	10.6
BM sm G90.1	393	19	111	0.3	0.0530	0.0007	0.051	0.001	0.358	0.006	0.016	0.001	329.0	4.6	320.4	5.0	310.9	5.3	312.8	15.3	2.6
BM lg G1.1	101	7	197	2.0	0.0586	0.0013	0.058	0.001	0.470	0.011	0.018	0.001	554.1	12.6	366.1	5.3	391.4	9.4	366.0	12.1	33.9
BM lg G7.1	440	21	63	0.1	0.0701	0.0016	0.049	0.001	0.444	0.012	0.039	0.002	930.4	20.7	309.2	4.2	373.2	9.7	764.4	44.6	66.8
BM lg G8.1	59	5	136	2.3	0.0559	0.0013	0.063	0.001	0.524	0.014	0.018	0.001	449.4	10.1	393.5	4.2	427.8	11.8	365.3	12.3	12.4
BM1g G11.1	396	31	197	0.5	0.1136	0.0016	0.066	0.001	0.981	0.017	0.057	0.003	1857.3	27.0	411.2	5.2	694.0	11.8	1129.0	55.6	77.9
BM1g G16.1	140	11	254	1.8	0.0809	0.0016	0.062	0.001	0.705	0.017	0.021	0.001	1218.3	24.3	386.8	5.1	541.6	12.9	428.9	14.3	68.2
BM1g G17.1	238	11	68	0.3	0.0545	0.0008	0.050	0.000	0.372	0.006	0.017	0.001	393.1	5.9	314.4	3.0	321.0	4.9	334.9	11.9	20.0
BM1g G21.1	1570	78	80	0.1	0.0681	0.0016	0.053	0.001	0.447	0.011	0.076	0.005	871.6	21.0	332.0	3.9	375.3	9.5	1477.5	100.3	61.9
BM1g G29.1	229	10	55	0.2	0.0527	0.0010	0.047	0.001	0.339	0.007	0.014	0.001	313.9	6.0	294.5	3.4	296.5	6.4	290.8	11.5	6.2
BM1g G26.1	364	20	104	0.3	0.0538	0.0007	0.059	0.001	0.426	0.007	0.018	0.001	362.2	4.7	369.9	4.2	360.3	6.0	351.1	11.6	-2.1
BM1g G31.1	98	5	40	0.4	0.0597	0.0018	0.058	0.001	0.505	0.020	0.021	0.001	592.0	17.4	365.4	8.7	415.1	16.7	423.1	28.7	38.3
BM1g G34.1	882	58	550	0.6	0.0584	0.0008	0.066	0.001	0.498	0.006	0.020	0.001	544.8	7.4	412.9	7.6	410.1	5.3	402.9	24.5	24.2
BM1g G40.1	109	7	31	0.3	0.0606	0.0015	0.065	0.001	0.552	0.018	0.026	0.003	625.7	15.3	404.7	7.9	446.1	14.3	515.5	50.9	35.3
BM1g G46.1	207	15	199	1.0	0.0803	0.0015	0.065	0.001	0.712	0.017	0.027	0.002	1205.2	23.0	405.8	7.8	546.2	13.2	533.1	34.4	66.3
BM1g G44.1	124	7	101	0.8	0.0559	0.0012	0.058	0.001	0.455	0.012	0.017	0.001	448.7	9.6	362.3	7.0	380.5	10.4	349.5	21.3	19.3
BM1g G63.1	980	49	109	0.1	0.0549	0.0007	0.056	0.001	0.380	0.007	0.030	0.003	409.9	5.5	350.6	7.4	327.0	5.8	607.0	51.1	14.5
BM1g G66.1	1337	81	83	0.1	0.1448	0.0044	0.055	0.001	1.022	0.035	0.278	0.016	2285.0	69.9	343.5	6.0	714.9	24.8	4955.0	282.8	85.0
BM1g G71.1	1689	419	46464	27.5	0.0708	0.0010	0.051	0.001	0.462	0.007	0.013	0.001	952.6	13.7	320.5	5.1	385.9	5.6	268.1	13.6	66.4
BM1g G73.1	77	4	44	0.6	0.0752	0.0020	0.056	0.001	0.595	0.023	0.024	0.001	1074.2	28.5	353.2	7.4	474.2	18.7	484.0	28.2	67.1
BM1g G76.1	300	15	52	0.2	0.0560	0.0008	0.051	0.001	0.381	0.006	0.018	0.001	453.3	6.6	321.9	5.1	327.6	5.2	357.5	19.9	29.0
BM1g G81.1	1433	76	450	0.3	0.0834	0.0021	0.053	0.001	0.547	0.014	0.035	0.003	1278.0	32.5	330.6	6.1	443.1	11.4	694.4	54.2	74.1

Table 2: Laser ablation ICPMS U–Pb-Th data and calculated ages for zircons from the Bodmin Moor granite, Cornwall.

St. Austell																					
	Concentrations				Ratios								Ages								
Samples	U (ppm)	Pb (ppm)	Th (ppm)	Th/U	$^{207}Pb/^{206}Pb$	1σ	$^{206}Pb/^{238}U$	1σ	$^{207}Pb/^{235}U$	1σ	$^{208}Pb/^{232}Th$	1σ	$^{207}Pb/^{206}Pb$	1σ Ma	$^{206}Pb/^{238}U$	1σ Ma	$^{207}Pb/^{235}U$	1σ Ma	$^{208}Pb/^{232}Th$	1σ Ma	Disc. %
SA sm G6.1	400	20	65	0.2	0.0780	0.0018	0.0466	0.0008	0.4605	0.0108	0.0355	0.0013	1147.7	26.0	293.6	5.3	384.6	9.0	705.5	26.8	74.4
SA sm G4.1	139	8	266	1.9	0.0574	0.0015	0.0459	0.0007	0.3591	0.0106	0.0144	0.0004	506.7	13.5	289.2	4.5	311.5	9.2	289.9	7.8	42.9
SA sm G15.1	63	4	105	1.7	0.0609	0.0026	0.0516	0.0009	0.4422	0.0207	0.0154	0.0005	636.5	27.6	324.4	5.9	371.8	17.4	309.1	10.1	49.0
SA sm G14.1	136	6	41	0.3	0.0564	0.0020	0.0447	0.0007	0.3423	0.0118	0.0113	0.0008	466.3	16.3	281.9	4.6	298.9	10.3	227.8	16.6	39.6
SA sm G13.2	333	16	105	0.3	0.0531	0.0010	0.0495	0.0007	0.3403	0.0070	0.0144	0.0005	334.2	6.5	311.4	4.4	297.4	6.2	288.2	10.4	6.8
SA sm G5.1	158	8	130	0.8	0.0609	0.0018	0.0484	0.0009	0.4032	0.0133	0.0182	0.0007	636.2	18.4	304.4	5.5	343.9	11.3	365.3	13.7	52.2
SA sm G17.1	252	12	118	0.5	0.0524	0.0012	0.0493	0.0006	0.3561	0.0087	0.0144	0.0004	303.1	6.7	310.2	4.1	309.3	7.5	289.0	9.0	-2.4
SA sm G18.1	142	9	143	1.0	0.1040	0.0028	0.0519	0.0010	0.7563	0.0223	0.0269	0.0009	1696.9	45.1	326.3	6.1	571.9	16.9	535.9	18.0	80.8
SA sm G20.1	175	11	61	0.3	0.1255	0.0035	0.0535	0.0011	0.9357	0.0295	0.0654	0.0026	2036.5	56.8	335.8	6.6	670.6	21.1	1279.8	50.8	83.5
SA sm G28.1	174	8	34	0.2	0.0552	0.0013	0.0497	0.0008	0.3678	0.0091	0.0185	0.0009	422.0	10.2	312.6	5.2	318.0	7.9	370.8	18.6	25.9
SA sm G29.1	250	12	82	0.3	0.0633	0.0014	0.0510	0.0008	0.4330	0.0124	0.0205	0.0008	717.6	15.7	320.7	4.9	365.3	10.4	409.6	16.3	55.3
SA sm G30.1	215	12	241	1.1	0.0951	0.0022	0.0489	0.0009	0.6326	0.0151	0.0215	0.0009	1530.6	35.5	308.0	5.7	497.7	11.9	430.9	17.5	79.9
SA sm G31.1	471	23	64	0.1	0.0527	0.0009	0.0532	0.0007	0.3324	0.0054	0.0152	0.0006	315.4	5.2	334.1	4.7	291.4	4.7	303.9	12.2	-6.0
SA sm G35.1	241	11	85	0.4	0.0639	0.0018	0.0460	0.0008	0.3883	0.0121	0.0127	0.0008	737.5	21.3	290.0	4.8	333.2	10.4	255.2	17.0	60.7
SA sm G40.1	342	17	52	0.2	0.0540	0.0009	0.0541	0.0007	0.3703	0.0071	0.0191	0.0008	370.7	6.4	339.4	4.3	319.9	6.1	381.8	15.8	8.5
SA sm G43.1	59	3	69	1.2	0.0770	0.0030	0.0488	0.0008	0.5307	0.0232	0.0184	0.0008	1120.1	44.1	307.2	5.1	432.3	18.9	368.1	15.6	72.6
SA sm G52.1	511	28	113	0.2	0.0571	0.0010	0.0549	0.0009	0.3708	0.0061	0.0310	0.0023	495.9	9.0	344.3	5.5	320.3	5.3	616.7	46.7	30.6
SA sm G57.1	129	6	78	0.6	0.0526	0.0015	0.0490	0.0008	0.3548	0.0094	0.0150	0.0006	313.5	8.7	308.2	5.0	308.3	8.2	300.7	11.9	1.7
SA sm G59.1	347	24	733	2.1	0.0916	0.0022	0.0519	0.0009	0.6372	0.0148	0.0188	0.0015	1459.0	34.6	326.1	5.5	500.6	11.6	376.1	29.2	77.6
SA sm G68.1	365	18	170	0.5	0.0532	0.0010	0.0506	0.0008	0.3572	0.0069	0.0140	0.0011	336.3	6.5	318.1	4.7	310.1	6.0	281.4	21.8	5.4
SA sm G66.1	251	12	83	0.3	0.0531	0.0011	0.0504	0.0008	0.3591	0.0070	0.0152	0.0012	334.7	7.0	317.0	4.9	311.6	6.1	304.1	24.4	5.3
SA sm G71.1	464	23	164	0.4	0.0576	0.0010	0.0526	0.0008	0.3949	0.0072	0.0193	0.0017	513.7	9.3	330.3	4.9	337.9	6.2	385.8	33.7	35.7
SA sm G61.1	515	27	468	0.9	0.0807	0.0017	0.0483	0.0008	0.5196	0.0095	0.0161	0.0012	1215.1	25.0	304.3	5.0	424.9	7.8	323.5	24.7	75.0
SA sm G74.1	55	3	62	1.1	0.0562	0.0022	0.0497	0.0009	0.4025	0.0196	0.0127	0.0010	460.1	18.4	312.7	5.8	343.5	16.7	255.1	20.4	32.0
SA lg G76.1	530	25	34	0.1	0.0508	0.0009	0.0507	0.0007	0.3384	0.0064	0.0129	0.0011	232.1	4.1	318.8	4.3	296.0	5.6	258.5	21.7	-37.4
SA lg G77.1	372	20	574	1.5	0.0564	0.0012	0.0482	0.0006	0.3679	0.0072	0.0135	0.0010	470.0	10.0	303.6	3.7	318.1	6.2	271.8	20.1	35.4
SA lg G79.1	525	25	158	0.3	0.0581	0.0010	0.0495	0.0006	0.3894	0.0058	0.0192	0.0015	533.4	8.7	311.7	3.6	333.9	5.0	384.7	29.1	41.6
SA lg G81.1	457	22	45	0.1	0.0652	0.0014	0.0487	0.0007	0.4374	0.0098	0.0543	0.0044	781.9	16.7	306.6	4.3	368.4	8.3	1069.2	86.5	60.8
SA lg G82.1	337	19	680	2.0	0.0530	0.0010	0.0470	0.0005	0.3523	0.0063	0.0115	0.0008	329.0	6.2	296.3	3.0	306.5	5.5	231.1	17.0	9.9
SA lg G83.1	425	20	349	0.8	0.0553	0.0010	0.0472	0.0004	0.3523	0.0057	0.0110	0.0008	424.4	7.8	297.4	2.7	306.5	5.0	221.6	16.3	29.9
SA lg G85.1	107	4	26	0.2	0.0686	0.0022	0.0382	0.0006	0.3608	0.0114	0.0270	0.0024	886.3	28.1	241.8	3.8	312.8	9.9	538.8	47.7	72.7
SA lg G86.1	307	15	163	0.5	0.0549	0.0012	0.0489	0.0005	0.3675	0.0077	0.0123	0.0009	408.2	8.6	307.6	2.9	317.8	6.7	248.0	18.7	24.6
SA lg G87.1	192	10	326	1.7	0.0743	0.0025	0.0434	0.0006	0.4455	0.0149	0.0172	0.0014	1048.4	35.5	274.1	3.9	374.1	12.5	345.1	27.3	73.9
SA lg G90.1	251	14	535	2.1	0.0542	0.0012	0.0460	0.0005	0.3398	0.0068	0.0116	0.0008	378.6	8.1	289.8	3.1	297.1	6.0	233.1	16.9	23.5
SA lg G91.1	535	26	464	0.9	0.0593	0.0011	0.0468	0.0006	0.3679	0.0057	0.0134	0.0010	576.8	10.4	294.6	3.9	318.1	4.9	269.5	19.7	48.9
SA lg G92.1	270	13	334	1.2	0.1146	0.0023	0.0385	0.0005	0.5987	0.0110	0.0214	0.0016	1872.9	38.3	243.4	3.1	476.4	8.8	428.4	31.8	87.0
SA lg G96.1	606	31	773	1.3	0.0546	0.0010	0.0492	0.0008	0.3551	0.0062	0.0109	0.0008	395.7	7.2	309.4	5.3	308.6	5.4	219.9	16.5	21.8
SA lg G99.1	423	24	971	2.3	0.0587	0.0012	0.0469	0.0008	0.3767	0.0077	0.0112	0.0008	557.0	11.7	295.5	5.0	324.6	6.7	224.2	16.7	46.9
SA lg G100.1	306	17	621	2.0	0.0539	0.0012	0.0469	0.0009	0.3485	0.0079	0.0115	0.0009	366.1	8.0	295.3	5.6	303.6	6.9	231.9	17.3	19.3
SA lg G100.2	2405	99	107	0.0	0.0550	0.0009	0.0458	0.0009	0.3196	0.0054	0.0193	0.0016	413.4	6.7	288.6	5.8	281.6	4.7	386.2	31.5	30.2
SA lg G104.1	2355	112	125	0.1	0.0524	0.0008	0.0523	0.0009	0.3496	0.0055	0.0136	0.0011	303.8	4.7	328.5	5.7	304.4	4.8	273.6	22.4	-8.2
SA lg G107.1	572	27	172	0.3	0.0523	0.0009	0.0498	0.0008	0.3469	0.0058	0.0123	0.0010	297.6	5.2	313.4	5.3	302.4	5.1	247.4	19.1	-5.3
SA lg G109.1	268	13	278	1.0	0.0574	0.0013	0.0465	0.0008	0.3723	0.0087	0.0120	0.0009	508.7	11.6	293.1	5.3	321.4	7.5	240.7	18.1	42.4
SA lg G110.1	736	34	200	0.3	0.0537	0.0010	0.0490	0.0008	0.3479	0.0063	0.0126	0.0010	358.2	6.6	308.5	4.9	303.1	5.5	253.9	19.6	13.9
SA lg G111.1	491	27	1033	2.1	0.0531	0.0012	0.0469	0.0007	0.3456	0.0089	0.0109	0.0006	334.9	7.4	295.7	4.3	301.4	7.8	218.5	12.2	11.7
SA lg G114.1	584	24	138	0.2	0.0525	0.0014	0.0437	0.0008	0.3173	0.0091	0.0088	0.0006	307.7	8.0	275.8	4.9	279.9	8.1	177.3	12.1	10.4
SA lg G119.1	538	24	287	0.5	0.0528	0.0011	0.0461	0.0007	0.3358	0.0085	0.0098	0.0006	320.9	7.0	290.6	4.2	294.0	7.4	196.6	11.1	9.5
SA lg G122.1	985	45	449	0.5	0.0572	0.0015	0.0472	0.0007	0.3561	0.0104	0.0095	0.0006	500.0	12.9	297.2	4.7	309.3	9.1	190.9	12.0	40.6
SA lg G116.1	1316	63	1167	0.9	0.0581	0.0012	0.0460	0.0007	0.3511	0.0086	0.0099	0.0006	533.5	11.3	290.1	4.2	305.6	7.5	198.8	11.3	45.6
SA lg G127.1	459	25	649	1.4	0.0614	0.0017	0.0475	0.0007	0.4091	0.0128	0.0117	0.0007	651.8	18.1	298.9	4.6	348.2	10.9	234.5	13.8	54.1
SA lg G128.1	338	17	488	1.4	0.0565	0.0014	0.0450	0.0007	0.3533	0.0099	0.0079	0.0005	471.7	11.8	284.0	4.1	307.2	8.6	158.5	9.3	39.8
SA lg G131.1	1008	46	64	0.1	0.0502	0.0010	0.0494	0.0007	0.3184	0.0075	0.0111	0.0007	203.2	4.1	310.6	4.6	280.7	6.6	222.2	14.1	-52.8
SA lg G143.1	3089	125	274	0.1	0.0555	0.0013	0.0428	0.0007	0.2952	0.0072	0.0171	0.0011	434.4	9.9	270.5	4.2	262.6	6.4	343.2	22.1	37.7
SA lg G140.1	949	42	137	0.1	0.0530	0.0011	0.0471	0.0006	0.3238	0.0077	0.0113	0.0007	327.8	6.8	296.8	4.1	284.8	6.8	227.4	13.5	9.4
SA lg G138.1	433	21	232	0.5	0.0496	0.0012	0.0481	0.0008	0.3285	0.0091	0.0089	0.0005	176.9	4.1	302.6	4.8	288.4	8.0	179.9	10.4	-71.1
SA lg G141.1	364	16	205	0.6	0.0627	0.0021	0.0446	0.0008	0.3847	0.0151	0.0107	0.0007	698.4	23.2	281.5	4.9	330.5	13.0	214.3	13.4	59.7

Table 3: Laser ablation ICPMS U–Pb-Th data and calculated ages for zircons from the St. Austell granite, Devon.

Carnmenellis																					
	Concentrations				Ratios								Ages								
Samples	U (ppm)	Pb (ppm)	Th (ppm)	Th/U	$^{207}Pb/^{206}Pb$	1σ	$^{206}Pb/^{238}U$	1σ	$^{207}Pb/^{235}U$	1σ	$^{208}Pb/^{232}Th$	1σ	$^{207}Pb/^{206}Pb$	1σ Ma	$^{206}Pb/^{238}U$	1σ Ma	$^{207}Pb/^{235}U$	1σ Ma	$^{208}Pb/^{232}Th$	1σ Ma	Disc. %
CARN lg G17.2	1041	56	133	0.1	0.0591	0.0010	0.0576	0.0007	0.3805	0.0076	0.0256	0.0022	572.0	10.1	360.9	4.3	327.4	6.5	511.2	43.0	36.9
CARN lg G16.1	240	11	69	0.3	0.0536	0.0013	0.0478	0.0007	0.3598	0.0093	0.0134	0.0011	353.5	8.3	301.3	4.1	312.1	8.1	269.6	22.0	14.8
CARN lg G15.1	83	5	70	0.8	0.0545	0.0016	0.0627	0.0010	0.4912	0.0172	0.0162	0.0013	391.2	11.8	392.1	6.0	405.8	14.2	325.2	26.6	-0.2
CARN lg G15.2	279	17	147	0.5	0.0565	0.0012	0.0607	0.0008	0.4715	0.0110	0.0164	0.0013	472.2	9.8	380.0	5.2	392.2	9.1	329.2	26.2	19.5
CARN lg G15.3	281	13	17	0.1	0.0523	0.0011	0.0518	0.0007	0.3655	0.0094	0.0155	0.0014	299.2	6.6	325.9	4.6	316.3	8.1	311.0	28.1	-8.9
CARN lg G14.1	1053	58	16	0.0	0.0545	0.0010	0.0599	0.0008	0.3651	0.0082	0.0569	0.0077	391.4	7.2	374.7	5.3	316.0	7.1	1119.4	151.2	4.2
CARN lg G12.2	843	46	24	0.0	0.0567	0.0013	0.0559	0.0009	0.3794	0.0091	0.0307	0.0030	478.0	10.7	350.4	5.6	326.6	7.9	610.5	59.2	26.7
CARN lg G11.1	279	16	108	0.4	0.0728	0.0018	0.0547	0.0011	0.5444	0.0149	0.0272	0.0022	1008.1	25.6	343.1	6.7	441.3	12.1	541.9	44.4	66.0
CARN lg G10.2	231	11	56	0.2	0.0634	0.0013	0.0477	0.0006	0.4126	0.0094	0.0222	0.0010	720.5	14.3	300.3	3.8	350.8	8.0	442.9	20.2	58.3
CARN lg G8.1	209	10	165	0.8	0.0692	0.0017	0.0452	0.0009	0.4341	0.0123	0.0165	0.0007	903.3	22.1	284.9	5.6	366.1	10.4	330.8	13.1	68.5
CARN lg G7.1	197	9	52	0.3	0.0548	0.0011	0.0487	0.0007	0.3667	0.0092	0.0178	0.0007	404.3	7.8	306.3	4.7	317.2	7.9	357.6	14.5	24.2
CARN lg G2.1	440	22	59	0.1	0.0574	0.0008	0.0536	0.0008	0.3720	0.0079	0.0232	0.0010	507.0	7.0	336.5	4.8	321.1	6.9	464.5	20.9	33.6
CARN lg G3.1	137	7	45	0.3	0.0562	0.0018	0.0566	0.0013	0.4249	0.0177	0.0181	0.0009	460.3	14.5	355.2	8.0	359.6	15.0	363.4	17.6	22.8
CARN lg G4.1	336	22	219	0.6	0.0721	0.0014	0.0622	0.0011	0.5919	0.0131	0.0244	0.0010	987.9	19.4	389.2	6.8	472.1	10.4	486.3	19.2	60.6
CARN lg G5.1	302	21	221	0.7	0.0566	0.0009	0.0677	0.0010	0.5199	0.0107	0.0198	0.0007	474.6	7.6	422.2	6.4	425.1	8.7	396.1	13.2	11.0
CARN lg G9.1	211	10	57	0.3	0.0525	0.0011	0.0505	0.0007	0.3607	0.0087	0.0150	0.0006	307.4	6.4	317.4	4.4	312.7	7.5	301.6	12.2	-3.3
CARN lg G18.1	198	9	33	0.2	0.0621	0.0016	0.0475	0.0014	0.3872	0.0116	0.0304	0.0020	679.0	18.0	299.0	9.1	332.3	10.0	604.7	39.7	56.0
CARN lg G18.2	193	9	36	0.2	0.0696	0.0016	0.0469	0.0007	0.4427	0.0118	0.0213	0.0008	915.6	20.4	295.7	4.7	372.1	9.9	426.4	16.6	67.7
CARN lg G19.1	185	9	39	0.2	0.0531	0.0010	0.0499	0.0006	0.3689	0.0091	0.0193	0.0007	331.9	6.2	313.9	3.9	318.8	7.8	386.4	14.8	5.4
CARN lg G20.1	25	2	20	0.8	0.0795	0.0039	0.0929	0.0017	0.9755	0.0398	0.0386	0.0020	1183.8	58.5	572.6	10.5	691.3	28.2	765.1	40.2	51.6
CARN lg G22.2	493	27	62	0.1	0.0639	0.0010	0.0541	0.0008	0.4242	0.0081	0.0476	0.0031	739.4	12.1	339.6	4.9	359.1	6.9	940.5	61.6	54.1
CARN sm G28.1	200	9	53	0.3	0.0526	0.0008	0.0492	0.0006	0.3591	0.0075	0.0142	0.0004	312.4	5.0	309.6	3.7	311.6	6.5	285.5	8.0	0.9
CARN sm G34.1	230	11	40	0.2	0.0515	0.0008	0.0498	0.0005	0.3510	0.0067	0.0146	0.0005	262.2	4.0	313.2	3.5	305.5	5.8	293.8	9.1	-19.4
CARN sm G35.1	739	48	255	0.3	0.1061	0.0021	0.0595	0.0009	0.7084	0.0173	0.0567	0.0017	1734.0	34.7	372.3	5.6	543.8	13.3	1115.6	33.0	78.5
CARN sm G37.1	104	6	109	1.0	0.0689	0.0020	0.0494	0.0007	0.4769	0.0171	0.0173	0.0011	895.4	25.8	311.0	4.4	396.0	14.2	347.4	23.0	65.3
CARN sm G38.1	58	17	26	0.4	0.1096	0.0015	0.2879	0.0035	4.4426	0.1173	0.0846	0.0055	1792.9	24.3	1631.3	19.8	1720.3	45.4	1641.4	106.0	9.0
CARN sm G36.1	469	25	126	0.3	0.0591	0.0009	0.0551	0.0007	0.3913	0.0082	0.0226	0.0015	570.1	8.9	346.1	4.6	335.3	7.0	451.4	30.4	39.3
CARN sm G39.1	88	4	77	0.9	0.0519	0.0014	0.0475	0.0006	0.3369	0.0099	0.0143	0.0009	280.3	7.3	299.2	3.8	294.8	8.7	286.9	18.8	-6.7
CARN sm G42.1	244	11	60	0.2	0.0590	0.0010	0.0486	0.0005	0.3908	0.0086	0.0187	0.0013	568.8	9.8	305.6	3.4	334.9	7.4	373.7	25.1	46.3
CARN sm G56.1	84	5	88	1.0	0.0852	0.0023	0.0512	0.0008	0.6040	0.0186	0.0249	0.0016	1321.2	35.0	322.1	5.2	479.8	14.8	497.6	32.8	75.6
CARN sm G61.1	465	26	187	0.4	0.0638	0.0010	0.0562	0.0007	0.4011	0.0085	0.0227	0.0015	733.5	11.7	352.5	4.1	342.5	7.2	452.8	30.0	51.9
CARN sm G123.1	178	8	39	0.2	0.0521	0.0010	0.0493	0.0007	0.3469	0.0084	0.0154	0.0013	289.1	5.5	310.1	4.3	302.4	7.3	308.6	26.0	-7.3
CARN sm G125.1	237	12	78	0.3	0.0519	0.0008	0.0505	0.0007	0.3624	0.0082	0.0167	0.0014	280.5	4.3	317.6	4.6	314.0	7.1	334.3	27.3	-13.2
CARN sm G126.1	165	8	34	0.2	0.0556	0.0012	0.0484	0.0007	0.3647	0.0100	0.0188	0.0016	435.5	9.3	304.9	4.1	315.8	8.7	377.1	31.7	30.0
CARN sm G127.1	113	7	22	0.2	0.0595	0.0012	0.0635	0.0009	0.5094	0.0146	0.0257	0.0022	585.2	11.8	396.8	5.6	418.0	12.0	513.8	43.6	32.2
CARN sm G128.1	481	25	120	0.2	0.0551	0.0007	0.0540	0.0007	0.3575	0.0070	0.0164	0.0013	415.6	5.4	339.2	4.6	310.4	6.0	328.8	26.7	18.4
CARN sm G132.1	430	22	74	0.2	0.0528	0.0007	0.0549	0.0008	0.3479	0.0066	0.0165	0.0013	320.1	4.1	344.6	5.0	303.1	5.8	330.6	27.0	-7.7
CARN sm G142.1	199	12	341	1.7	0.0609	0.0018	0.0480	0.0009	0.3933	0.0143	0.0164	0.0014	634.6	18.5	302.0	5.5	336.7	12.3	329.3	27.4	52.4
CARN sm G141.1	106	18	77	0.7	0.0926	0.0016	0.1548	0.0021	1.9756	0.0476	0.0680	0.0056	1478.9	26.1	928.1	12.6	1107.2	26.7	1329.2	108.8	37.2
CARN sm G147.1	455	24	120	0.3	0.0571	0.0007	0.0532	0.0008	0.3652	0.0070	0.0171	0.0014	495.0	6.2	334.2	5.0	316.1	6.1	342.4	28.6	32.5
CARN sm G136.1	315	15	71	0.2	0.0543	0.0008	0.0501	0.0006	0.3540	0.0073	0.0157	0.0013	382.6	5.8	315.2	4.0	307.7	6.3	314.7	25.9	17.6
CARN sm G138.1	172	8	61	0.4	0.0674	0.0014	0.0488	0.0007	0.4478	0.0119	0.0232	0.0019	850.2	17.6	307.4	4.4	375.7	10.0	464.2	38.9	63.8
CARN sm G137.1	290	14	66	0.2	0.0518	0.0008	0.0495	0.0007	0.3302	0.0075	0.0146	0.0012	277.8	4.4	311.5	4.2	289.7	6.6	293.6	24.7	-12.1

Table 4: Laser ablation ICPMS U–Pb-Th data and calculated ages for zircons from the Carnmenellis granite, Cornwall.

Land's End																					
	Concentrations				Ratios								Ages								
Samples	U (ppm)	Pb (ppm)	Th (ppm)	Th/U	$^{207}Pb/^{206}Pb$	1σ	$^{206}Pb/^{238}U$	1σ	$^{207}Pb/^{235}U$	1σ	$^{208}Pb/^{232}Th$	1σ	$^{207}Pb/^{206}Pb$	1σ Ma	$^{206}Pb/^{238}U$	1σ Ma	$^{207}Pb/^{235}U$	1σ Ma	$^{208}Pb/^{232}Th$	1σ Ma	Disc. %
LE sm G22.1	727	37	322	0.4	0.0644	0.0012	0.0532	0.0011	0.4257	0.0103	0.0150	0.0014	754.1	14.6	334.4	6.8	360.1	8.7	301.8	28.5	55.6
LE lg G15.1	813	37	111	0.1	0.0548	0.0007	0.0483	0.0006	0.3330	0.0059	0.0155	0.0006	406.0	5.3	304.3	4.0	291.8	5.2	311.5	12.2	25.1
LE lg G14.1	371	17	35	0.1	0.0540	0.0008	0.0476	0.0006	0.3431	0.0070	0.0143	0.0006	370.8	5.8	299.9	3.8	299.5	6.1	287.7	11.6	19.1
LE lg G4.1	332	15	29	0.1	0.0524	0.0009	0.0475	0.0006	0.3318	0.0072	0.0167	0.0007	304.9	5.1	299.3	3.6	291.0	6.3	334.8	14.3	1.8
LE sm G15.1	732	33	178	0.2	0.0721	0.0014	0.0468	0.0009	0.4258	0.0089	0.0233	0.0022	988.3	19.0	294.5	5.6	360.2	7.5	464.7	44.1	70.2

Table 5: Laser ablation ICPMS U–Pb-Th data and calculated ages for zircons from the Land's End granite, Cornwall.

Method	LA-ICPMS - this study				TIMS - Chesley et al. (1993)				TIMS - Chen et al. (1993)			
Pluton	*Age*	*2σ*	*Min*	*Location*	*Age*	*2σ*	*Min*	*Location*	*Age*	*2σ*	*Min*	*Location*
Bodmin Moor Granite (BMG)	316	4	Zr	De Lank	291.4	0.8	Mz	Brockabarrow Common	281.4	0.6	Mz	De Lank
St Austell Granite (SAG)	305	5	Zr	Luxulyan	281.8	0.4	Mz	Luxulyan (n=3)	280.3	0.8	Mz	Luxulyan
Carnmenellis Granite (CG)	313	3	Zr	Rosemanowes	294.0	1.0	Mz	Bosahan	293.7	0.8	Mz	Carnsew
Land's End Granite (LEG)	300	5	Zr	Castle-an-Dinas	279.2	0.6	Xe	Castle-an-Dinas	277.0	0.6	Mz	Castle-an-Dinas

Pb207/U235 ages quoted throughout

Table 6: Comparsion of LA-ICPMS U–Pb zircon ages (this study) with those from TIMS U–Pb monazite / xenotime (Chesley et al., 1993; Chen et al., 1993).

	Bodmin Moor Outer	**Bodmin Moor Inner**	**Carnmenellis Outer**	**Carnmenellis Inner**
wt %				
SiO_2	71.31	71.73	72.11	72.84
TiO_2	0.24	0.14	0.24	0.18
Al_2O_3	15.14	14.79	15.04	14.64
Fe_2O_3	1.93	1.32	1.60	1.47
MgO	0.40	0.24	0.43	0.39
CaO	0.75	0.56	0.92	0.68
Na_2O	2.79	2.81	3.06	3.19
K_2O	5.42	5.41	5.12	4.95
Zr (ppm)	88.00	57.00	109.00	74.00
M	1.04	1.03	1.10	1.08
T_{Zr} (°C)	**761.25**	**727.29**	**775.10**	**744.38**

Table 7: Average chemical analyses of the Bodmin Moor and Carnmenellis granites, from Stone (2000). Calculations for M and T calculated using equations from Watson & Harrison (1983) and Miller et al. (2003).